Journal of Computational Physics **150,** 332–372 (1999)
Article ID jcph.1999.6184, available online at http://www.idealibrary.com on IDEAL®

The Lattice Solid Model to Simulate the Physics of Rocks and Earthquakes: Incorporation of Friction

David Place and Peter Mora[1]

QUAKES, The University of Queensland, Brisbane, 4072 Queensland, Australia
E-mail: place@earthsciences.uq.edu.au and mora@earthsciences.uq.edu.au

Received June 16, 1997; revised November 11, 1998

The particle-based lattice solid model developed to study the physics of rocks and the nonlinear dynamics of earthquakes is refined by incorporating intrinsic friction between particles. The model provides a means for studying the causes of seismic wave attenuation, as well as frictional heat generation, fault zone evolution, and localisation phenomena. A modified velocity–Verlat scheme that allows friction to be precisely modelled is developed. This is a difficult computational problem given that a discontinuity must be accurately simulated by the numerical approach (i.e., the transition from static to dynamical frictional behaviour). This is achieved using a half time step integration scheme. At each half time step, a nonlinear system is solved to compute the static frictional forces and states of touching particle-pairs. Improved efficiency is achieved by adaptively adjusting the time step increment, depending on the particle velocities in the system. The total energy is calculated and verified to remain constant to a high precision during simulations. Numerical experiments show that the model can be applied to the study of earthquake dynamics, the stick–slip instability, heat generation, and fault zone evolution. Such experiments may lead to a conclusive resolution of the heat flow paradox and improved understanding of earthquake precursory phenomena and dynamics.

Key Words: friction; earthquakes; nonlinear dynamics; lattice solid model; particle-based model; heat of earthquakes; fault gouge; numerical simulation; rock physics; heat flow paradox.

[1] Affiliations: SSA, AGU, AAAS, SEG.

0021-9991/99 $30.00

INTRODUCTION

The "lattice solid model" (Mora [14]) consists of a lattice of interacting particles and was motivated by short range molecular dynamics concepts. In the model, particles represent grains of rock and interactions are specified accordingly. The model was developed in order to study fracturing (Mora and Place [15]), wave propagation in complex discontinuous media, faulting (Donzé *et al*. [7]) and the stick–slip instability which is responsible for earthquakes (Mora and Place [16]).

In the initial version, only elastic interactions in which particles of a model rock matrix were linked by elastic–brittle bonds were specified. Despite the simplicity of the interactions, realistic stick–slip frictional behaviour was observed during numerical experiments involving two elastic–brittle blocks with rough surfaces being pushed past one another at a constant rate. During the "stick" phase, the stress in the solid built up until two interlocking asperities of the fault pushed past one another, releasing some of the stress, initiating slip of the two blocks, and exciting a slip pulse which propagated along the fault. During the propagation of the slip pulse, fault normal motions were observed. The results show that even using simple elastic interactions the model was capable of reproducing stick–slip frictional behaviour and slip pulses compatible with those measured in field and laboratory experiments.

A long standing paradox in earthquake studies has been the low heat flow observed around the San Andreas fault compared with the theoretical value computed using the value of rock friction measured in laboratory experiments. To explain this paradox, Brune *et al*. [3] proposed that slip occurs during the passage of interface waves which locally reduce the normal stress as they propagate along the fault. Numerical experiments (Mora and Place [16]) using the lattice solid model have demonstrated the existence of slip pulses with particle motions normal to the fault, similar to those observed by Brune and co-workers [3] in stick–slip experiments involving foam rubber blocks. Early lattice solid simulations did not model intrinsic friction between particles or heat generation so it was not possible to determine whether the fault normal motions during the propagation of slip pulses were sufficient to explain the heat flow paradox.

The lattice solid model was therefore extended to incorporate a simple intrinsic friction between particles and to simulate heat generation. Additional computations required to incorporate the effect of friction necessitated further refinement of the model.

In order to quantitatively study heat generation and to simulate frictional behaviour (including the transition between static and dynamical behaviour), frictional forces must be "accurately" computed and the discontinuity between static and dynamical behaviour must be modelled. Heat is generated when two surfaces are slipping past one another (i.e., the frictional behaviour is dynamic). When the surfaces are locked (i.e., the frictional behaviour is static) no heat should be generated. Hence, the model is based on the assumption that if two surfaces are locked by static friction, the slip velocity between these two surfaces is zero (measured as the slip velocity between surface particles). The transition between static and dynamic frictional behaviour is also an important consideration. Due to the time discretisation, only linear processes can be simulated within a finite time step, so one takes discontinuities into account when going from one time step to the next. However, within a time step discontinuities may occur and one must take them into account before proceeding to the next time step. Ignoring these discontinuities (that is, assuming that they occur only at the instant between two time steps) can yield incorrect frictional behaviour.

In this paper, we develop an approach, the lattice solid approach, that seeks the static frictional force such that no slip is allowed when two surfaces are locked by static friction. The approach consists of solving a nonlinear system to compute the effective frictional forces that must be applied during a time step. Frictional forces are computed such that the transition between static and dynamic behaviour is captured within a time step by introducing an intermediate state in which particles are bouncing (when the direction of the slip reverses but the slip does not stop), starting to slip, or stopping. The precision with which the lattice solid approach computes static frictional forces, defined as the amount of slip between surface particles that are locked by static friction, is compared to the precision of two other methods. The first is based on a simple iterative method that attempts to capture the transition between static and dynamic behaviour and was first used in studies of the effect of intrinsic friction on the dynamics of earthquakes (Mora and Place [17], Place and Mora [22]). The second method is based on the Distinct Element Model proposed by Cundall and Strack [6], which provides a simple and natural way to compute frictional forces. Comparisons involve determining how closely energy remains constant during the simulation and calculating a heat error term that relates to the amount of slip observed between particles locked by static friction.

LATTICE SOLID MODEL

The particles in the lattice solid model, like the particles in short range molecular dynamics, interact with each other. However, particles represent grains or units of rock that may range from grain size to tens of metres in diameter. Particles are used as the building blocks of grains of rocks. The smallest indivisible unit of the system is specified by groupings of several strongly bonded particles. These groups can be considered as idealised unbreakable grains or units of rock. This approach enables the nonlinear behaviour of discontinuous solids to be simulated with relative simplicity.

LATTICE STRUCTURE

On the scale of a laboratory experiment in which rock friction is studied, particles in the model represent grain-sized units of rock. Particles are arranged in a regular two dimensional triangular lattice and linked by breakable bonds (Fig. 1). Although rocks are discontinuous at many scales (e.g., rocks contain both micro- and macro-fractures and are made up of

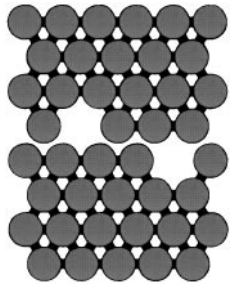

FIG. 1. Closeup of a 2D close-packed lattice of bonded particles with a horizontal fault. The fault is specified as an irregularly shaped rupture in the lattice in which particles on the upper block are not bonded to particles on the lower block.

grains with different chemical compositions), isotropic elasticity is a good approximation for rock behaviour in the small strain macroscopic limit. In the macroscopic limit and assuming radial pairwise particle interactions, the triangular lattice solid structure has the elastic properties of an isotropic solid with a compressional wave speed $\sqrt{3}$ times the shear wave speed (Aki and Richards [1, p. 4]), very similar to that of typical crustal rocks. The disadvantage of such a regular structure is that the fracture behaviour is anisotropic (Mora and Place [15]) and would be more comparable to that of a pure crystal. In order to enable isotropic fracturing behaviour to be modelled more like that of rock, different particle sizes or a random lattice should be used (Christ *et al.* [5]).

GRAINS AND PARTICLES

To enable isotropic fracturing and to obtain more realistic behavior at the smallest scale in the model, particles are grouped into "grains" of different sizes and shapes. Bonds, linking particles inside a grain, are set to be much stronger than bonds that link particles belonging to different grains (i.e., grains are made of material stronger than the overall strength of the material being modelled). Grains can be considered the smallest indivisible units of the system. Rotational dynamics is simulated at the grain scale as a consequence of linear momentum conservation of the bonded particles in a grain although it is not modelled at the particle scale. Furthermore, this kind of grouping of particles into grains allows isotropic fracturing to be modelled. This is because grains can be made of a variable number of particles, and hence have different sizes and shapes.

Grains of rocks are deformed when subjected to a shear stress. These deformations can be modelled at the particle scale by introducing a "soft" shear constraint at the particle scale (i.e., the particle has a shear elasticity). This approach has been developed by Cundall and co-workers [6] and introduces a shear stiffness at the particle scale. The shear stiffness should be chosen such that the elastic properties of a granular medium relative to those of an equivalent bonded system of grains remain unchanged (i.e., such that Poisson's ratio σ of the solid being modelled is $\sigma \sim 1/3$, as for real rocks). In our model, a "rigid" shear constraint is used. Hence particles are rigid and cannot be deformed when subjected to shear stress. By grouping particles to form grains, shear deformations can effectively take place because bonds inside a grain are stretched or compressed.

Because the smallest indivisible unit of the system is now composed of several particles, this approach requires a large number of particles to simulate the same number of grains of rock. Typically, 128×128 particles are used, and, in order to have a sufficient number of grains, the grains are composed of only a small number of particles (e.g., 3 to 10 particles). Also typically, four different shapes of grains of model rock are used: elongated hexagon (composed of 10 particles), hexagon (7 particles), diamond (4 particles), and triangle (3 particles).

SIMPLE PARTICLE INTERACTIONS WITHOUT INTRINSIC FRICTION

Particles are bonded by linear elastic bonds that break when the separation exceeds a given threshold. This is expressed through a parabolic potential function that is radially dependent (Fig. 2, Eq. (1)). When a given separation (r_{break}) is reached, the bond breaks irreversibly. When the bond is broken, particles are free to move apart and only the repulsive part of the interaction remains unchanged (i.e., the potential function becomes a half parabola).

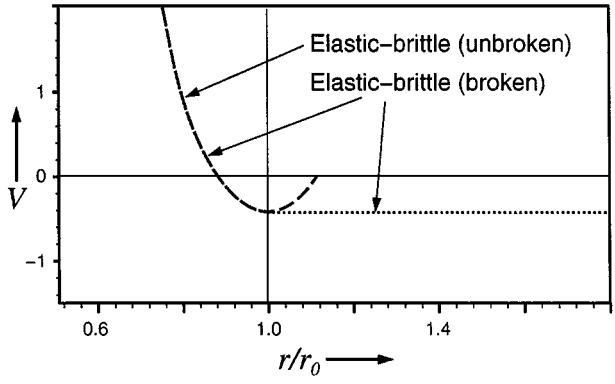

FIG. 2. Effective inter-particle potential. Bonded particles (dashed line) repel one another when the separation is less than the equilibrium separation r_0, and attract one another when the separation is greater than r_0. Unbonded particles (dotted line) repel one another when the separation is less than r_0 and do not interact when the separation is greater than r_0.

The potential function described above is specified as

$$V(r) = \begin{cases} V_0 + \frac{1}{2}k(r - r_0)^2, & r \leq R \\ V(R), & r > R, \end{cases} \tag{1}$$

where k is the spring constant of the bond and r_0 is the equilibrium separation. The range R where the potential becomes flat is given by

$$R = R(t) = \begin{cases} r_{break}, & r(\tau) < r_{break} \text{ for all } \tau < t \\ r_0, & \text{otherwise,} \end{cases} \tag{2}$$

where the radial separation r is computed using

$$r = r_{nm} = |\mathbf{x}_n - \mathbf{x}_m|, \tag{3}$$

$$V_0 = -\tfrac{1}{2}k(r_{break} - r_0)^2, \tag{4}$$

with $\mathbf{x}_n$ and $\mathbf{x}_m$ respectively denoting the positions of particle n and particle m and t denoting the current time.

Different values for the breaking separation r_{break} are used to specify material with different strengths, with values typically ranging from $1.01r_0$ to $1.5r_0$ (i.e., much higher than the range of breaking criteria under dilation for macroscopic failure of rocks). A value of $1.5r_0$ is used to inhibit fracture and focus only on studying the effect of friction, elastic interaction, and fault geometry. A high value of the breaking separation is also used to prevent grains from breaking down into single particles that may interact "unrealistically" with other grains (single particles have an infinite shear stiffness, unlike grains of real rock, and are not allowed to rotate). Unbreakable material may also be used to prevent formation of a fault gouge if, for instance, the goal of the simulation is to study only the effect of surface roughness and/or intrinsic friction.

The elastic force on particle n is given by the sum of all pair forces

$$\mathbf{F}_n^I = \sum_{m \neq n} \mathbf{F}_{nm}^{(2)}. \tag{5}$$

The force on particle n due to a particle m for a given spring constant k is

$$\mathbf{F}_{nm}^{(2)} = \begin{cases} -k(r - r_0)\mathbf{e}_r, & r \leq R \\ 0, & r > R, \end{cases} \tag{6}$$

where the unit vector pointing from particle m to particle n is

$$\mathbf{e}_r = \frac{\mathbf{x}_n - \mathbf{x}_m}{r}. \tag{7}$$

An artificial viscosity is added to damp the reflected waves from the rigid edges of the lattice and to avoid buildup of kinetic energy in the closed system. The viscosity is frequency independent and does not fundamentally alter the dynamics of the system if carefully chosen (Mora and Place [16]). The total force on particle n is

$$\mathbf{F}_n = \mathbf{F}_n^I + \mathbf{F}_n^v, \tag{8}$$

where the viscous force is given by

$$\mathbf{F}_n^v = -\nu\dot{\mathbf{x}}_n. \tag{9}$$

INTRINSIC FRICTION

Early simulations using the lattice solid model (without intrinsic friction) have shown that the model is capable of simulating the stick–slip instability and slip pulses. However, since heat generation was not modelled, questions such as Can the slip pulse locally reduce the normal stress sufficiently to explain the anomalously low heat flow observed around the San Andreas fault? could not be answered. Heat in real solids relates to quantised lattice vibrations (kinetic energy) at the microscopic scale. These lattice vibrations are generated when microscopically rough surfaces slip past one another. Roughness at the microscopic scale (at the particle scale for the model) can be modelled using a "friction law." Hence we incorporate an intrinsic friction at the particle scale to model heat generation. Heat is then defined as the work done by intrinsic friction.

When two grain surfaces are in contact and slipping past one another, a dynamic frictional force opposes the direction of slip. The two surfaces stop slipping when the external forces that cause the surfaces to slip no longer exceed the dynamic frictional forces. Then, the two surfaces are locked by static friction. We are interested in modelling frictional processes of faults, and we decided to be demanding with regard to modelling of static friction. When two surfaces are locked by static friction, no slip is allowed between surfaces before the shear force overcomes the static friction. Frictional forces are applied at the surface particle centres and not at the surface of the surface particles where the contact actually occurs (this effectively means that frictional forces exert slightly less torque than they should, making it harder to rotate grains). Slip velocity between grain surfaces is computed as the slip velocity between the centres of mass of surface particles that are in contact. Three different approaches for modelling this kind of frictional interaction will be discussed in the next section.

A simple intrinsic friction corresponding to Coulomb friction is added to the model when two surface particles that are not bonded come in contact (i.e., repel one another). For a given

intrinsic frictional coefficient μ, a tangential acceleration a_{ij}^d due to the dynamic frictional force between the particles i and j is computed, and its direction is opposite that of the tangential movement between particles. If the tangential acceleration required to stop slip between particles after one time step is greater than the dynamic acceleration a_{ij}^d, then the two particles are allowed to slip and the acceleration due to the dynamic frictional force (Ma_{ij}^d) is applied. Otherwise, particles are locked by a static frictional force which is lower than the dynamic frictional force and must be determined.

The dynamic frictional acceleration used here is velocity independent and is proportional to the normal force (stress) between particles, namely

$$a_{ij}^d = \mu \frac{k}{M} \frac{r_0 - r_{ij}}{r_0}, \tag{10}$$

where M is the particle mass. The total acceleration of particle n resulting from all elastic and frictional interactions is given by

$$\ddot{\mathbf{x}}_i(t) = \ddot{\mathbf{x}}_i^0(t) + \sum_{l \in P_i} \ddot{\mathbf{x}}_{il}^F(t), \tag{11}$$

where P_i denotes the set of unbonded particles interacting with particle i, $\ddot{\mathbf{x}}_{il}^F$ is the effective frictional acceleration for particle-pair il due to the dynamic or static frictional force, and $\ddot{\mathbf{x}}_i^0(t)$ denotes the value of the acceleration before the frictional acceleration is added. This elastic acceleration is given by

$$\ddot{\mathbf{x}}_n^0(t) = \frac{\mathbf{F}_n(t)}{M}. \tag{12}$$

The tangential velocity $\dot{x}_{ij}^T$ and acceleration $\ddot{x}_{ij}^T$ of a particle-pair ij are computed relative to the midpoint of the particle-pair and are respectively given by

$$\dot{x}_{ij}^T(t) = (\dot{\mathbf{x}}_i(t) - \dot{\mathbf{x}}_j(t)) \cdot \mathbf{e}_{ij}^T, \tag{13}$$

and

$$\ddot{x}_{ij}^T(t) = (\ddot{\mathbf{x}}_i(t) - \ddot{\mathbf{x}}_j(t)) \cdot \mathbf{e}_{ij}^T, \tag{14}$$

where particle velocities ($\dot{\mathbf{x}}_i$) are updated using a modified velocity–Verlat scheme, described in the next section. The tangential unit vector of particle-pair ij, denoted $\mathbf{e}_{ij}^T$, is given by

$$\mathbf{e}_{ij}^T = \frac{\dot{\mathbf{x}}_{ij} - (\dot{\mathbf{x}}_{ij} \cdot \mathbf{e}_r)\mathbf{e}_r}{|\dot{\mathbf{x}}_{ij} - (\dot{\mathbf{x}}_{ij} \cdot \mathbf{e}_r)\mathbf{e}_r|}, \tag{15}$$

with $\dot{\mathbf{x}}_{ij}$ defined as

$$\dot{\mathbf{x}}_{ij} = \dot{\mathbf{x}}_i - \dot{\mathbf{x}}_j. \tag{16}$$

Before one computes the effective frictional acceleration ($\ddot{\mathbf{x}}_{il}^F$) in Eq. (11), the numerical integration (to compute particle velocities and positions) must be cast in such a way that one can compute the frictional forces that take into account discontinuities that may occur during a time step (i.e., bond breaking yields a discontinuity in force), as does the transition between dynamic and static frictional behaviour.

HALF TIME STEP INTEGRATION

The numerical integration is based on a velocity–Verlat scheme (Allen and Tildesley [2]) given by

$$\mathbf{x}_n(t+\Delta t) = \mathbf{x}_n(t) + \Delta t\dot{\mathbf{x}}_n(t) + \frac{\Delta t^2}{2}\ddot{\mathbf{x}}_n(t), \tag{17}$$

$$\dot{\mathbf{x}}_n(t+\Delta t) = \dot{\mathbf{x}}_n(t) + \Delta t\frac{\ddot{\mathbf{x}}_n(t) + \ddot{\mathbf{x}}_n(t+\Delta t)}{2}, \tag{18}$$

where the velocity is updated using the value of the acceleration at the middle of the time step (computed by averaging the accelerations at the beginning and end of the time step). The velocity–Verlat scheme assumes that accelerations are continuous during a time step. Due to bond breaking, a discontinuity may occur during the time step. Bonds are forced to break exactly at time t, when the displacements are computed, in order to capture the discontinuity precisely. Therefore, the elastic force changes at time t if bond breaking has occurred. In other words, the elastic accelerations ($\ddot{\mathbf{x}}_n^0$) at $t-\epsilon$ (denoted t^-) and $t+\epsilon$ (denoted t^+) are different. As the static frictional forces depend on all other forces acting on particles, this discontinuity in elastic forces includes a discontinuity in frictional forces. Hence, different elastic and frictional forces must be applied at $t-\epsilon$ and $t+\epsilon$. This is achieved using a half time step integration approach in which the time step is centred on t. Forcing bond breaking to occur at time t in the model (i.e., the middle of the time step) allows the effect of delaying the fracture as a result of the time discretisation to be minimised. With a full time step integration, bonds will be broken at $t+\frac{\Delta t}{2}$ just before one proceeds to the next time step. Hence, the interactions would have been computed as if the bond were unbroken. Therefore the half time step integration allows the discontinuity to be captured more precisely without using a smaller time step interval.

A full time step goes from $t-\frac{\Delta t}{2}$ to $t+\frac{\Delta t}{2}$, where the particle positions are updated at t and particle accelerations are computed at t^- and t^+. The particle positions and velocities are consequently updated using

$$\mathbf{x}_n(t+\Delta t) = \mathbf{x}_n(t) + \Delta t\dot{\mathbf{x}}_n(t) + \frac{\Delta t^2}{2}\ddot{\mathbf{x}}_n(t^+), \tag{19}$$

$$\dot{\mathbf{x}}_n(t+\Delta t) = \dot{\mathbf{x}}_n(t) + \Delta t\frac{\ddot{\mathbf{x}}_n(t^+) + \ddot{\mathbf{x}}_n(t^- + \Delta t)}{2}. \tag{20}$$

We can write the updating of velocities as

$$\dot{\mathbf{x}}_n\left(t+\frac{\Delta t}{2}\right) = \dot{\mathbf{x}}_n(t) + \frac{\Delta t}{2}\ddot{\mathbf{x}}_n(t^+), \tag{21}$$

$$\dot{\mathbf{x}}_n(t+\Delta t) = \dot{\mathbf{x}}_n\left(t+\frac{\Delta t}{2}\right) + \frac{\Delta t}{2}\ddot{\mathbf{x}}_n(t^- + \Delta t), \tag{22}$$

or equivalently,

$$\dot{\mathbf{x}}_n(t) = \dot{\mathbf{x}}_n\left(t-\frac{\Delta t}{2}\right) + \frac{\Delta t}{2}\ddot{\mathbf{x}}_n(t^-), \tag{23}$$

$$\dot{\mathbf{x}}_n\left(t+\frac{\Delta t}{2}\right) = \dot{\mathbf{x}}_n(t) + \frac{\Delta t}{2}\ddot{\mathbf{x}}_n(t^+), \tag{24}$$

where $\ddot{\mathbf{x}}_n(t^-)$ and $\ddot{\mathbf{x}}_n(t^+)$ are the particle accelerations before and after bond breaking. We express these two steps using a single equation as

$$\dot{\mathbf{x}}_n(\tau + \Delta\tau) = \dot{\mathbf{x}}_n(\tau) + \Delta\tau\ddot{\mathbf{x}}_n(T), \tag{25}$$

where $\Delta\tau = \frac{\Delta t}{2}$ and

$$T = \begin{cases} t^+, & \tau = t \\ t^-, & \tau = t - \frac{\Delta t}{2}. \end{cases} \tag{26}$$

The forces due to the viscosity are computed at time t when the velocity is known.

VISCOSITY

The half time step velocity–Verlat scheme requires the values of the particle accelerations at t^- in order to update the particle velocities at time t (cf. Eq. (23)). The accelerations are computed from the frictional forces, elastic forces, and viscous forces (Eqs. (11), (12), and (8)). The viscous forces are computed using Eq. (9), which requires the values of the particle velocities. To summarise, in order to update the particle velocities at time t, the viscous forces at time t must be computed, but these require the values of particle velocities at time t. Consequently, the forces due to the artificial viscosity are computed using an iterative algorithm. Table I specifies the algorithm used when elastic and viscous forces only are modelled. Incorporation of artificial viscosity during modelling of frictional forces will be discussed in the next section.

COMPUTATION OF FRICTIONAL FORCES

Before describing our numerical approach, we will consider two simple methods of computing frictional forces. The purpose of the frist one is to compute a value for the frictional force that precisely stops slip between particles in static frictional contact; the second method is based on the Distinct Element Model proposed by Cundall and co-workers [6, 8]. A detailed comparison between our approach and the two methods is shown in the Appendix.

TABLE I
Computation of Viscous Forces

do for all particles n
$\quad \mathbf{F}_n^v(t) = -\nu\dot{\mathbf{x}}_n(t)$
$\quad \ddot{\mathbf{x}}_n^0(t^-) = \frac{1}{M}\left(\mathbf{F}_n^I(t^-) + \mathbf{F}_n^v(t)\right)$
$\quad \dot{\mathbf{x}}_n(t) = \dot{\mathbf{x}}_n\left(t - \frac{\Delta t}{2}\right) + \frac{\Delta t}{2}\ddot{\mathbf{x}}_n^0(t^-)$
until *converged*

Note. The elastic forces are computed at $t - \epsilon$ (denoted $\mathbf{F}_n^I(t^-)$) before bonds are broken.

A SIMPLE APPROACH

The following approach is based on the assumption that one can isolate and solve the frictional interaction between two particles without considering frictional interactions with other particles. Once elastic and viscous forces acting on each particle are known, the frictional forces are applied. This is done assuming that there will be no change in external forces (that is, all forces including frictional forces that act on a particle) while the frictional forces are applied. As the other frictional forces acting on a given particle do change the external force acting on it, iterations are needed. The "simple" iterative method consists of computing the "static" acceleration required to stop slip between particles during a half time step $\Delta\tau = \frac{\Delta t}{2}$. The tangential velocity (given by Eqs. (25) and (13)) at the end of the half time step will be

$$\dot{x}_{ij}^T(\tau + \Delta\tau) = \dot{x}_{ij}^T(\tau) + \Delta\tau\left((\mathbf{a}_{ex})_{ij}(T) + \ddot{\mathbf{x}}_{ij}^F(T)\right) \cdot \mathbf{e}_{ij}^T, \tag{27}$$

where the effective total acceleration due to all forces, excluding the frictional force on pair ij, is

$$(\mathbf{a}_{ex})_{ij}(T) = \ddot{\mathbf{x}}_i^0(T) + \sum_{l \in P_i, l \neq j} \ddot{\mathbf{x}}_{il}^F(T). \tag{28}$$

Therefore, the static frictional acceleration $a_{ij}^s(T)$ that should be applied to stop slip between particle i and particle j during a half time step interval $\Delta\tau$ is calculated by setting $\dot{x}_{ij}^T(\tau + \Delta\tau) = 0$ and $\ddot{\mathbf{x}}_{ij}^F(T) = a_{ij}^s(T)\mathbf{e}_{ij}^T$ in Eq. (27), yielding

$$a_{ij}^s(T) = -\frac{\dot{x}_{ij}^T(\tau)}{\Delta\tau} - (\mathbf{a}_{ex})_{ij}(T) \cdot \mathbf{e}_{ij}^T. \tag{29}$$

The effective frictional acceleration ($\ddot{\mathbf{x}}_{ij}^F$) is computed as the minimum of the static and dynamic acceleration using

$$\ddot{\mathbf{x}}_{ij}^F(T) = a_{ij}^F(T)\mathbf{e}_{ij}^T, \tag{30}$$

and

$$a_{ij}^F(T) = \begin{cases} -\frac{\dot{x}_{ij}^T(\tau)}{\left|\dot{x}_{ij}^T(\tau)\right|}\left|a_{ij}^d(T)\right|, & \left|a_{ij}^s(T)\right| > \left|a_{ij}^d(T)\right| \\ a_{ij}^s(T), & \text{otherwise,} \end{cases} \tag{31}$$

where a_{ij}^F denotes the magnitude of the effective or applied frictional acceleration. The applied frictional accelerations are computed by iterating Eqs. (29) and (31), starting from $a_{ij}^F = 0$, until convergence is achieved (no further change in a_{ij}^F within a specified precision).

Unfortunately, this method is not stable because this approach assumes that forces acting on a particle ($M\mathbf{a}_{ex}$) will not change while the frictional forces are applied. When the frictional forces are applied to a particle i, the forces acting on all particles that are in contact with this particle change. Since these changes in forces are not considered, the algorithm cannot "exactly" stop slip between particles locked by static friction. This results in oscillation between the dynamic and static states when the values of static frictional forces are close to the dynamic value. Hence, the transition between dynamic and static behaviour is not accurately modelled. Instabilities are manifested as oscillations during the

iterative procedure of particle-pairs between static and dynamic states (cf. the Appendix). When complex interactions are involved, the oscillations of particle-pair states result in non-convergence of the iterative algorithm.

CUNDALL APPROACH

In the lattice solid model, particles have a radial intrinsic elasticity that results in a normal elastic force between interacting particles. Hence, a "normal stiffness" is introduced at the particle scale and shear stiffness of a system of particles is a consequence of the geometric arrangement of the triangular lattice. The triangular lattice has a shear modulus $\lambda = \frac{\sqrt{3}}{4}k$ (Mora and Place [16]). The numerical approach proposed by P. A. Cundall applies the same principle to shear forces at the particle scale in a granular medium interacting through friction. In his model, two unbonded particles undergo elastic shear restoring forces until these exceed a given threshold (Ma_{ij}^d) and the particles are allowed to slip. Therefore, a "shear stiffness" is effectively introduced at the particle scale that may modify the macroscopic elastic properties of a given structure. In contrast, unbonded particles in static frictional contact in the simple iterative approach described previously would be seen as having an infinite shear stiffness.

The "shear stiffness" introduced at the particle scale can be seen as the shear deformation occurring when two particles are locked by static friction. When the surfaces of two particles are locked, the particles can be deformed, and hence slip will occur if this is measured as the displacement between the two particle centres. The use of the "soft" shear constraint on particles introduces an error due to the time discretisation: frictional forces are computed from the particle displacement since the last time step. During the next time step, the frictional forces applied may be too large or too small for the given time step increment and may result in a change in the particle frictional behaviour (going from static to dynamic frictional behaviour, for instance). Thus, transitions between static and dynamic frictional behaviour may be delayed by up to a time step and transition between static and dynamic states can incorrectly occur. In the Cundall approach, frictional forces also include the restoring shear forces due to the particle elasticity. The fact that the frictional force does not oppose the direction of slip is not indicative of an error in that case. However, changes in frictional behaviour may occur when one restores forces due to the particle shear elasticity changes (caused by overestimating or underestimating the frictional forces during a time step) while the frictional force at the particle surface should remain static or dynamic. Hence, the ability to capture the frictional discontinuity (changes between the static and dynamic states) depends on the time step increment. In contrast, use of a "rigid" shear constraint and the lattice solid approach allows the frictional behaviour within a time step to be captured more precisely. Hence we choose to use a "rigid" shear constraint at the particle scale. In comparing the lattice solid approach and the "Cundall approach," this will require use of infinite shear stiffness in Cundall's method.

The resulting shear force in Cundall's method is computed by accumulating variations in shear forces using

$$\mathbf{F}_{ij}^s(T + \Delta\tau) = \mathbf{F}_{ij}^s(T) + \Delta\mathbf{F}_{ij}^s(T), \tag{32}$$

where

$$\Delta\mathbf{F}_{ij}^s(T) = -K_s\Delta\mathbf{U}_{ij}^s(T) \tag{33}$$

and

$$\Delta \mathbf{U}_{ij}^{s}(T) = \Delta\tau \dot{x}_{ij}^{T}(\tau)\,\mathbf{e}_{ij}^{T}, \tag{34}$$

and K_s denotes the joint stiffness (stress/displacement). The frictional acceleration is computed from the shear force and is given by

$$\ddot{\mathbf{x}}_{ij}^{F}(T) = a_{ij}^{F}(T)\,\mathbf{e}_{ij}^{T}, \tag{35}$$

where

$$a_{ij}^{F}(T) = \begin{cases} \dfrac{a_{ij}^{s}(T)}{\left|a_{ij}^{s}(T)\right|}\left|a_{ij}^{d}(T)\right|, & \left|a_{ij}^{s}(T)\right| > \left|a_{ij}^{d}(T)\right| \\ a_{ij}^{s}(T), & \text{otherwise,} \end{cases} \tag{36}$$

and

$$a_{ij}^{s}(T) = \frac{1}{M}\mathbf{F}_{ij}^{s}(T)\cdot\mathbf{e}_{ij}^{T}. \tag{37}$$

This approach provides a stable, simple, and efficient way to compute the frictional forces. To accurately simulate (under the given assumptions of our current model) static frictional behaviour, slip between the surface particles of grains must be exactly stopped when the contact is static. The joint stiffness K_s in the Cundall approach introduces a "soft" shear constraint. To exactly stop slip between particles when the contact is static, the shear constraint must be rigid, and hence the joint stiffness K_s must be infinite. As a result, (cf. the Appendix) the transition between static and dynamic behaviour is not precisely captured using a finite time step and a joint stiffness K_s ranging from 1 to 50 times k. This is manifested as slip between supposedly static particles. As explained previously, the use of a "soft" shear constraint causes the frictional forces to be underestimated or overestimated, thereby resulting in the possibility of incorrect transitions between static and dynamic frictional behaviour. The lower the joint stiffness, the higher the underestimate or overestimate of the frictional force. To capture the frictional discontinuity more precisely, a large value of K_s must be used (i.e., particles are given greater shear rigidity). However, to ensure numerical stability and accuracy, the time step increment must be chosen such that

$$\Delta\tau < 2c\sqrt{\frac{M}{2K_s}}, \tag{38}$$

where c is a user-defined factor (typically, $c = 0.1$, depending on the number of contacts that a particle can have simultaneously). Therefore a very small time step increment must be used to obtain a precise computation of frictional forces such that slip between static pairs is stopped, which results in excessively costly calculations.

A PRECISE NUMERICAL APPROACH (LATTICE SOLID APPROACH)

The computation of the frictional forces using the lattice solid approach consists of accurately modelling discontinuities in the frictional behaviour (i.e., transition between static and dynamic frictional behaviour) and solving for frictional forces by simultaneously considering all interactions between particle-pairs. Slip between particles is stopped if

particles are "static." As in the iterative method described previously, this implies that particles in static frictional contact have an infinite shear rigidity. In order to obtain elastic behaviour similar to that of rocks, particles are grouped to form grains which represent the smallest indivisible unit of the system. Hence grains in the model can be deformed when subjected to shear or normal stress similarly to grains of rock. Slip between surface particles that are in contact are "exactly" stopped (the slip velocity between the particle centres is zero) if the frictional behaviour is static.

Because of our interest in precisely simulating static frictional behaviour in the proposed model, shear interactions of surface particles (prior to slip) are rigid, while normal interactions are "soft." Since particles are always bonded with at least two other particles to form a piece of model material or grain (i.e., the smallest grain is roughly triangular shaped), what would have been seen as "rigid" shear interactions if one were at a particle scale will actually be a "soft" interaction between grains (as a consequence of the imposition of elastic shear resistance by the lattice geometry as the grains distort). In other words, shear interactions between grains of model rock are "soft" not by definition at the particle scale but as an emergent property.

This model therefore provides an approach more precise (under the given assumptions of our current model) than the approaches of the two methods outlined previously (iterative and Cundall approaches).

MODELLING FRICTIONAL DISCONTINUITIES

A particle-pair is "static" when the tangential velocity is zero; otherwise the particle-pair is "dynamic." Due to the time discretisation, particles may undergo a transition between static and dynamic behavior during a time interval $\Delta\tau$. Therefore three more states are distinguished (Fig. 3). The first two states are "stopping," where particle-pairs are changing

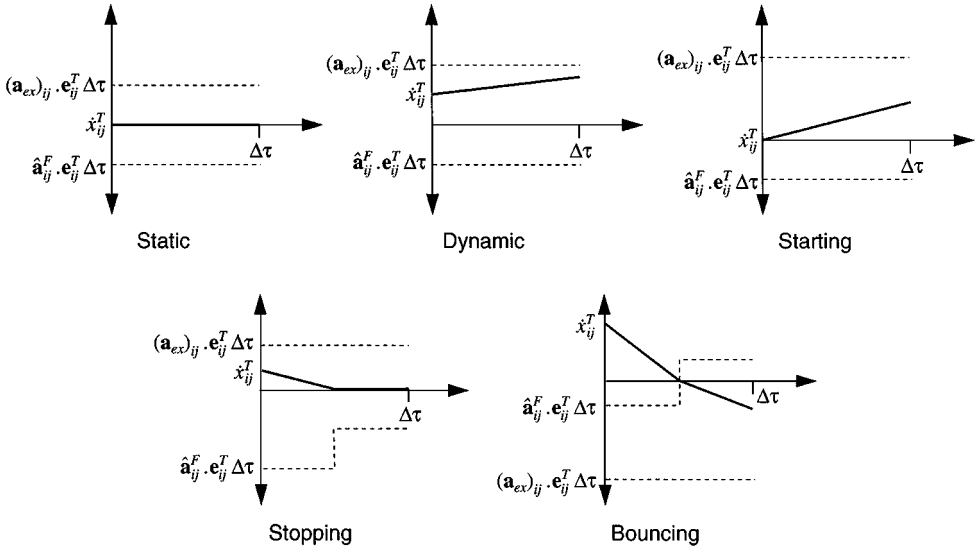

FIG. 3. Theoretical dynamics of the five different particle-pair states, where $\dot{x}_{ij}^T$ denotes the relative tangential velocity between the particles i and j, $\hat{\mathbf{a}}_{ij}^F$ denotes the theoretical frictional acceleration, and $(\mathbf{a}_{ex})_{ij}$ denotes the external accelerations due to all forces excluding this frictional force. The theoretical accelerations are those of the true dynamics corresponding to the five states that must be modelled.

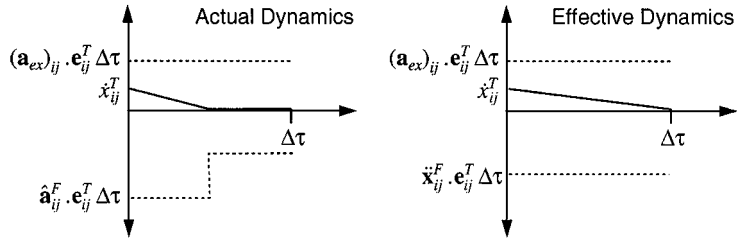

FIG. 4. Dynamics of stopping particle-pairs, where $\dot{x}_{ij}^T$ denotes the relative tangential velocity between the particles i and j, $\hat{\mathbf{a}}_{ij}^F$ denotes the actual or theoretical frictional acceleration, and $(\mathbf{a}_{ex})_{ij}$ denotes the external accelerations due to all forces except this frictional force $\ddot{\mathbf{x}}_{ij}^F$. Shown are actual or desired dynamics (left) and effective dynamics (right) that yield an equivalent configuration (velocity) to the true dynamics at the end of the half time step.

from dynamic to static, and "starting," where particle-pairs are changing from static to dynamic. The last state concerns dynamic particle-pairs with a tangential velocity that changes in sign during the time interval $\Delta\tau$ (the slip between the two particles does not stop but the tangential velocity is zero at some instant during the half time step). These are termed "bouncing" particle-pairs.

The time discretisation requires that all applied or "effective" forces be constant during a time interval $\Delta\tau$: when the velocity from the acceleration is updated using the modified velocity–Verlat scheme (Eq. (22)), the velocity obtained for the half time step is the one obtained for a constant acceleration. Thus, we seek the effective frictional accelerations $\ddot{\mathbf{x}}_{ij}^F$ which yield the same dynamics (i.e., final velocity) as the theoretical frictional acceleration $\hat{\mathbf{a}}_{ij}^F$ depicted in Fig. 3. For static particle-pairs, the frictional force is constant and equals the force required to maintain the particle-pair static during the half time step and hence $\ddot{\mathbf{x}}_{ij}^F = -(\mathbf{a}_{ex})_{ij}$. Dynamic and starting particle-pairs have (by definition) a constant frictional acceleration equal to the dynamic frictional acceleration (a_{ij}^d). Hence, the magnitude of the effective frictional acceleration for dynamic and starting particle-pairs is $|\ddot{\mathbf{x}}_{ij}^F| = |\hat{\mathbf{a}}_{ij}^F| = a_{ij}^d$. Stopping particle-pairs are static exactly at the end of the half time step, which is achieved by applying an effective frictional force equal to the force required to stop slip between the particles at the end of the time interval $\Delta\tau$ (Fig. 4). This effective frictional force, which depends on $(\mathbf{a}_{ex})_{ij}$ and the tangential velocity at the start of the time interval, must be determined.

For bouncing particle-pairs, the effective frictional force is the weighted average of forces which should be applied before and after the tangential velocity passes through zero (Fig. 5),

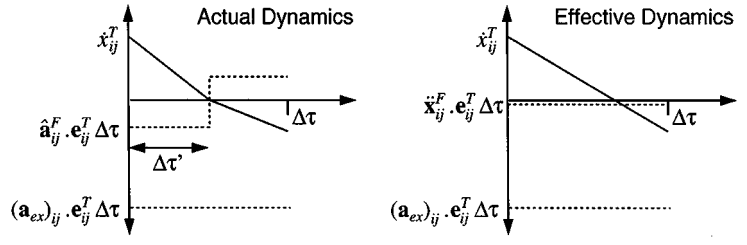

FIG. 5. Dynamics of bouncing particle-pairs, where $\dot{x}_{ij}^T$ denotes the relative tangential velocity between the particles i and j, $\hat{\mathbf{a}}_{ij}^F$ denotes the actual or theoretical frictional acceleration, and $(\mathbf{a}_{ex})_{ij}$ denotes the external accelerations due to all forces except this frictional force. Shown are actual or desired dynamics (left) and effective dynamics (right) that yield an equivalent configuration (velocity) to the true dynamics at the end of the half time step.

thus yielding the same final velocity that would result from application of the true frictional force,

$$\begin{aligned}\dot{x}^T(\tau+\Delta\tau) &= \dot{x}^T(\tau) + \Delta\tau\left(\ddot{\mathbf{x}}_{ij}^F(T) + (\mathbf{a}_{ex})_{ij}(T)\right)\cdot\mathbf{e}_{ij}^T \\ &= \dot{x}^T(\tau) + \Delta\tau\left(\frac{\Delta\tau'}{\Delta\tau}\hat{\mathbf{a}}_{ij}^F(T) + \frac{\Delta\tau-\Delta\tau'}{\Delta\tau}\hat{\mathbf{a}}_{ij}^F(T+\Delta\tau') + (\mathbf{a}_{ex})_{ij}(T)\right)\cdot\mathbf{e}_{ij}^T,\end{aligned} \tag{39}$$

where T is given by Eq. (26), $\tau+\Delta\tau'$ is the instant when the tangential velocity reaches zero, and $\hat{\mathbf{a}}_{ij}^F(T)$ and $\hat{\mathbf{a}}_{ij}^F(T+\Delta\tau')$ are respectively the true frictional forces that must be applied before and after the tangential velocity passes through zero. The effective frictional acceleration for bouncing particle-pairs is consequently given by

$$\ddot{\mathbf{x}}_{ij}^F(T) = \frac{\Delta\tau'}{\Delta\tau}\hat{\mathbf{a}}_{ij}^F(T) + \frac{\Delta\tau-\Delta\tau'}{\Delta\tau}\hat{\mathbf{a}}_{ij}^F(T+\Delta\tau'). \tag{40}$$

From the above, it is evident that effective frictional accelerations for static, stopping, and bouncing particle-pairs depend on the frictional accelerations of other pairs ($(\mathbf{a}_{ex})_{ij}$). Hence, the effective frictional accelerations must be computed simultaneously. The effective frictional accelerations of static and stopping particle-pairs are defined as the accelerations required for the tangential velocity at $\tau+\Delta\tau$ to reach zero. This definition of static pairs allows them to be treated identically to stopping particle-pairs and avoids the possibility that the tangential velocities will drift from zero due to numerical roundoff error accumulation. Therefore, if bouncing particles could be ignored, frictional forces for static, stopping, dynamic, and starting particle-pairs would be computed simultaneously by applying the dynamic frictional acceleration (a_{ij}^d) for starting and dynamic particle-pairs and then computing the frictional accelerations for static and starting particle-pairs such that

$$\dot{x}_{ij}^T(\tau+\Delta\tau) = 0. \tag{41}$$

In order to treat bouncing particle-pairs simultaneously with the other particle-pairs, we define $\tau+\Delta\tau'$ as the instant when the tangential velocity reaches zero. The effective frictional force for bouncing particle-pairs is computed from $\Delta\tau'$, the dynamic acceleration, and the initial velocity (Fig. 5). Therefore, the frictional acceleration for bouncing particle-pairs is defined as the acceleration required for the tangential velocity at $\tau+\Delta\tau'$ to reach zero. For static and stopping particles we set $\Delta\tau'=\Delta\tau$. Hence, the frictional forces of all particle-pairs are computed simultaneously by defining the effective frictional acceleration as the acceleration required for the tangential velocity at $\tau+\Delta\tau'$ to reach zero, namely

$$\dot{x}_{ij}^T(\tau+\Delta\tau') = 0. \tag{42}$$

In order to solve Eq. (42), the value of $\Delta\tau'$ for bouncing particle-pairs must be obtained. This value is computed such that the modified velocity–Verlat scheme using a half time step integration (Eq. (25)) is verified. The particle velocity, given by

$$\dot{\mathbf{x}}_i(\tau+\Delta\tau) = \dot{\mathbf{x}}_i(\tau) + \Delta\tau\left[(\mathbf{a}_{ex})_{ij}(T) + \ddot{\mathbf{x}}_{ij}^F(T)\right], \tag{43}$$

equals the velocity that would have been computed at the next half time step using the "exact" equations in which the frictional forces from τ to $\tau+\Delta\tau'$ (denoted $\hat{\mathbf{a}}_{ij}^F(T)$) and

from $\tau + \Delta\tau'$ to $\tau + \Delta\tau$ (denoted $\hat{\mathbf{a}}_{ij}^F(T + \Delta\tau')$) are equal in magnitude and opposite in sign:

$$\dot{\mathbf{x}}_i(\tau + \Delta\tau') = \dot{\mathbf{x}}_i(\tau) + \Delta\tau' \left[(\mathbf{a}_{ex})_{ij}(T) + \hat{\mathbf{a}}_{ij}^F(T) \right], \tag{44}$$

$$\dot{\mathbf{x}}_i(\tau + \Delta\tau) = \dot{\mathbf{x}}_i(\tau + \Delta\tau') + (\Delta\tau - \Delta\tau') \left[(\mathbf{a}_{ex})_{ij}(T + \Delta\tau') + \hat{\mathbf{a}}_{ij}^F(T + \Delta\tau') \right], \tag{45}$$

where $(\mathbf{a}_{ex})_{ij}$ is defined by Eq. (28) and is given by

$$(\mathbf{a}_{ex})_{ij}(T) = (\mathbf{a}_{ex})_{ij}(T + \Delta\tau'). \tag{46}$$

The exact or theoretical frictional force $\hat{\mathbf{a}}_{ij}^F$ is given by

$$\hat{\mathbf{a}}_{ij}^F(T) = -\hat{\mathbf{a}}_{ij}^F(T + \Delta\tau') = -\frac{\dot{x}_{ij}^T(\tau)}{\left|\dot{x}_{ij}^T(\tau)\right|} a_{ij}^d(T)\, \mathbf{e}_{ij}^T. \tag{47}$$

From the previous equations, the value of $\Delta\tau'$ relates to $\ddot{\mathbf{x}}_{ij}^F$ and $\hat{\mathbf{a}}_{ij}^F$ through

$$\Delta\tau' = \Delta\tau'_{ij} = \frac{\Delta\tau}{2} \left(\frac{\ddot{\mathbf{x}}_{ij}^F(T) \cdot \mathbf{e}_{ij}^T}{\hat{\mathbf{a}}_{ij}^F(T) \cdot \mathbf{e}_{ij}^T} + 1 \right). \tag{48}$$

NONLINEAR SYSTEM TO COMPUTE EFFECTIVE FRICTIONAL ACCELERATION

For a given particle-pair state, the effective frictional acceleration of the dynamic and starting particle-pairs is equal to the dynamic acceleration a_{ij}^d (computed using Eq. (10)), which opposes the tangential velocity. The effective frictional accelerations for the static, stopping, and bouncing pairs must be computed by solving these accelerations such that Eq. (42) is verified. Since the directions of the frictional accelerations are known for these pairs, only the magnitudes a_{ij}^s must be computed. Using Eqs. (11), (13), and (20), one may write Eq. (42) as a nonlinear system involving all stopping, static, and bouncing particle-pairs ij, namely

$$\mathbf{q}(\mathbf{a}^s) = \begin{bmatrix} \vdots \\ \dot{x}_{ij}^T(\tau + \Delta\tau') \\ \vdots \end{bmatrix} = \begin{bmatrix} \vdots \\ 0 \\ \vdots \end{bmatrix}, \tag{49}$$

where

$$\mathbf{a}^s = \begin{bmatrix} \vdots \\ a_{ij}^s \\ \vdots \end{bmatrix}, \tag{50}$$

and

$$\dot{x}_{ij}^T(\tau + \Delta\tau') = \dot{x}_{ij}^T(\tau) + \Delta\tau' a_{ij}^T(T), \tag{51}$$

$$a_{ij}^T(T) = a_{ij}^0(T) + \sum_{l \in P_i} \ddot{\mathbf{x}}_{il}^F(T) \cdot \mathbf{e}_{ij}^T - \sum_{l \in P_j} \ddot{\mathbf{x}}_{jl}^F(T) \cdot \mathbf{e}_{ij}^T, \tag{52}$$

$$a_{ij}^0(T) = \left(\ddot{\mathbf{x}}_i^0(T) - \ddot{\mathbf{x}}_j^0(T) \right) \cdot \mathbf{e}_{ij}^T, \tag{53}$$

with the expression $\Delta\tau'$ given by Eq. (48). This quadratic system can be solved using a Newton algorithm by iteratively solving the equation

$$(\mathbf{a}^s)_n = (\mathbf{a}^s)_{n-1} - (\nabla\mathbf{q}_{n-1})^{-1}\mathbf{q}_{n-1}, \tag{54}$$

which can be written using the form $\mathbf{Ax}+\mathbf{b}=0$ as

$$\nabla\mathbf{q}_{n-1} \times (\mathbf{a}^s)_n + \mathbf{b} = 0, \tag{55}$$

where

$$\mathbf{b} = \mathbf{q}_{n-1} - \nabla\mathbf{q}_{n-1} \times (\mathbf{a}^s)_{n-1}, \tag{56}$$

and $(\mathbf{a}^s)_n$ denotes the frictional acceleration of all stopping, starting, and bouncing particle-pairs at the nth iteration of the Newton algorithm, and $\mathbf{q}_n$ is equal to $\mathbf{q}((\mathbf{a}^s)_n)$ (i.e., the value of $\mathbf{q}$ at the nth iteration). The derivative of $\mathbf{q}_{n-1}$ is given by

$$\nabla\mathbf{q}_{n-1} = \begin{bmatrix} \vdots & \\ \cdots & \frac{\partial q_{ij}}{\partial a^F_{lm}} \quad \cdots \\ \vdots & \end{bmatrix}, \tag{57}$$

where, from Eq. (51),

$$\begin{aligned} \frac{\partial q_{ij}}{\partial a^s_{lm}} &= \frac{\partial \Delta\tau'}{\partial a^s_{lm}} a^T_{ij} + \Delta\tau' \frac{\partial a^T_{ij}}{\partial a^s_{lm}} + \frac{\partial \dot{x}^T_{ij}}{\partial a^s_{lm}}, \\ &= \frac{\partial \Delta\tau'}{\partial a^s_{lm}} a^T_{ij} + \Delta\tau' \frac{\partial a^T_{ij}}{\partial a^s_{lm}}, \end{aligned} \tag{58}$$

and by Eq. (52),

$$\frac{\partial a^T_{ij}}{\partial a^s_{lm}} = \begin{cases} \mathbf{e}^T_{lm} \cdot \mathbf{e}^T_{ij}, & l = i \\ -\mathbf{e}^T_{lm} \cdot \mathbf{e}^T_{ij}, & l = j \\ 0, & \text{otherwise}, \end{cases} \tag{59}$$

and

$$\frac{\partial \Delta\tau'}{\partial a^s_{lm}} = \begin{cases} 0, & \text{state} = \text{static or stopping} \\ \frac{\Delta\tau}{2\hat{\mathbf{a}}^F_{ij}(T) \cdot \mathbf{e}^T_{ij}}, & \text{state} = \text{bouncing}, \end{cases} \tag{60}$$

from the expression of $\Delta\tau'$ given by Eq. (48). The initial value of $\mathbf{a}^s$, denoted $(\mathbf{a}^s)_0$, is set to the static frictional acceleration computed for the previous time step. In order to compute $\nabla\mathbf{q}_{n-1}$ and proceed to the next iteration of the Newton algorithm (cf. Table II), the values of $\hat{\mathbf{a}}^F_{ij}$, $\Delta\tau'$, and a^T_{ij} must be updated. Therefore, the effective frictional acceleration

TABLE II
Computation of the Effective Frictional Accelerations for a Given Fixed State and Viscous Forces

Set particle-pair state to the last computed state
Set frictional accelerations to the last computed frictional accelerations
do
  Apply the effective frictional forces (Eq. (11))
  Update the tangential velocities $\dot{x}_{ij}^T(\tau + \Delta\tau)$ (Eqs. (25) and (13))
  Computer $\Delta\tau'$ (Eq. (48))
  Update the tangential velocities $\dot{x}_{ij}^T(\tau + \Delta\tau')$ (Eqs. (44) and (13))
  Compute the effective tangential accelerations a_{ij}^T (Eq. (62))
  Compute $\nabla \mathbf{q}_{n-1}$ (Eq. (57))
  Proceed to the next iteration of the Newton algorithm
  Compute the frictional accelerations (a_{ij}^s) by solving the linear system (55)
  Compute the effective frictional accelerations (Eq. (61))
until *converged*

$\ddot{\mathbf{x}}_{ij}^F$ is updated according to new estimations of a_{ij}^s for all static, stopping, and bouncing particle-pairs:

$$\ddot{\mathbf{x}}_{ij}^F = \begin{cases} a_{ij}^s \cdot \mathbf{e}_{ij}^T, & \text{state} = \text{static, stopping, or bouncing} \\ \text{unchanged}, & \text{state} = \text{dynamic or starting.} \end{cases} \tag{61}$$

The values of $\hat{\mathbf{a}}_{ij}^F$ and $\Delta\tau'$ are subsequently updated by respectively using Eqs. (47) and (48). Finally, the tangential velocities at $\tau + \Delta\tau'$ ($\dot{x}_{ij}^T(\tau + \Delta\tau')$) must be recomputed using Eqs. (44) and (13) in order to update a_{ij}^T using

$$a_{ij}^T = \frac{\dot{x}_{ij}^T(\tau + \Delta\tau') - \dot{x}_{ij}^T(\tau)}{\Delta\tau'}, \tag{62}$$

which can be deduced from Eq. (51).

The iterative Newton algorithm is specified in Table II, where computation of the effective friction forces is shown. The convergence criterion is based on the error of the slip velocity for static and bouncing particle-pairs at $\tau + \Delta\tau$, which should be zero. Namely, convergence is achieved if

$$\dot{x}_{ij}^T(\tau + \Delta\tau) < \epsilon_s, \tag{63}$$

where ϵ_s is chosen according to the specific computer's numerical precision (typically $\epsilon_s = 10^{-18}$ in double precision).

Particle-pair states are set before the Newton algorithm shown in Table II is performed, and they remain unchanged until the algorithm converges. Therefore the resulting effective frictional acceleration may not be consistent with that of the particle-pair states. For instance, the frictional acceleration required to stop slip between two particles may be so great that the particle-pair state should be dynamic rather than static. Hence, the particle-pair states must also be updated in accordance with the computed values of a_{ij}^s.

PARTICLE-PAIRS STATE ITERATIVE PROCEDURE

The states of particle-pairs are determined from the frictional accelerations a_{ij}^s and the tangential velocities. Particle-pair states are determined using

$$\text{State} = \begin{cases} \text{static}, & \dot{x}_{ij}^T(\tau) = 0 \;\&\; a_{ij}^s < a_{cut} \\ \text{starting}, & \dot{x}_{ij}^T(\tau) = 0 \;\&\; a_{ij}^s \geq a_{cut} \\ \text{stopping}, & \dot{x}_{ij}^T(\tau) \neq 0 \;\&\; a_{ij}^s < a_{cut} \\ \text{dynamic}, & \dot{x}_{ij}^T(\tau)\dot{x}_{ij}^T(\tau + \Delta\tau) \geq 0 \;\&\; a_{ij}^s \geq a_{cut} \\ \text{bouncing}, & \dot{x}_{ij}^T(\tau)\dot{x}_{ij}^T(\tau + \Delta\tau) < 0 \;\&\; a_{ij}^s \geq a_{cut}, \end{cases} \tag{64}$$

where a_{cut} is such that the frictional acceleration never exceeds the dynamic frictional acceleration (i.e., $\hat{\mathbf{a}}_{ij}^F \cdot \mathbf{e}_{ij}^T \leq a_{ij}^d$). From Eq. (40) the value of a_{cut} is given by

$$a_{cut} = (a_{cut})_{ij} = \begin{cases} \left(\frac{2\Delta\tau_{ij}'}{\Delta\tau} - 1\right) a_{ij}^d, & \text{last computed state} = \text{bouncing} \\ a_{ij}^d, & \text{otherwise.} \end{cases} \tag{65}$$

Particle-pair tangential velocities at $\tau + \Delta\tau$ ($\dot{x}_{ij}^T(\tau + \Delta\tau)$) are updated using Eq. (25). The effective frictional acceleration $\ddot{\mathbf{x}}_{ij}^F$ is computed using

$$\ddot{\mathbf{x}}_{ij}^F = \begin{cases} a_{ij}^s \mathbf{e}_{ij}^T, & \text{state} = \text{static or stopping} \\ a_{ij}^d \mathbf{e}_{ij}^T, & \text{state} = \text{starting or dynamic} \\ \left(\frac{2\Delta t'}{\Delta\tau} - 1\right) a_{ij}^d \mathbf{e}_{ij}^T, & \text{state} = \text{bouncing.} \end{cases} \tag{66}$$

The effective frictional accelerations are consequently modified after the particle-pair states have been updated. Hence, frictional interactions have changed and the effective frictional forces must be recomputed. This is achieved using an iterative procedure (Table III) which recomputes the frictional forces and updates the particle states until there is no further change in the particle-pair states, the effective frictional accelerations have converged within some tolerance, and Eq. (63) is verified.

The initial particle-pair states and the frictional accelerations are respectively set to the states and the frictional accelerations computed at the previous time step for particle-pairs

TABLE III
Computation of the Effective Frictional Acceleration

Set the particle-pair state to the state computed at the previous time step
Set the frictional acceleration to the values computed at the previous time step
do
  Update of the effective frictional accelerations (Table II kernel)
  Apply effective frictional force (Eq. (11))
  Update tangential velocities $\dot{x}_{ij}^T(\tau + \Delta\tau)$ (Eqs. (25) and (13))
  Update particle-pair states (Eq. (64))
  Update effective frictional accelerations (Eq. (66))
until *converged*

TABLE IV
Computation of Forces due to Friction and Viscosity on Unbonded Touching Particles

do for all particles n **in frictional interaction**
- $\mathbf{F}_n^v(t) = -\nu\dot{\mathbf{x}}_n(t)$
- $\ddot{\mathbf{x}}_n^0(t^-) = \frac{1}{M}\left(\mathbf{F}_n^I(t^-) + \mathbf{F}_n^v(t)\right)$
- Update effective frictional accelerations (Table III kernel)
- $\ddot{\mathbf{x}}_n(t^-) = \ddot{\mathbf{x}}_n^0(t^-) + \sum_{l\in P_n}\ddot{\mathbf{x}}_{nl}^F(t^-)$
- $\dot{\mathbf{x}}_n(t) = \dot{\mathbf{x}}_n\left(t - \frac{\Delta t}{2}\right) + \frac{\Delta t}{2}\ddot{\mathbf{x}}_n(t^-)$

until *converged*

remaining in contact. For particles coming into contact, the state is set to "dynamic" and the frictional acceleration is set to a_{ij}^d (N.B. The choice of the initial state affects only the rate of convergence of the algorithm.) Non-convergence can occur when the matrix $\nabla\mathbf{q}$ becomes numerically irregular. In that case, frictional forces may be incorrect. When non-convergence occurs, the frictional forces are corrected such that their direction is opposite the direction of slip and they do not exceed the dynamic frictional force. Non-convergence occurs only under a specific arrangement of particles, where, in the worst case, we have observed that one non-convergence occurs every 100,000 time steps and affects less than 0.1% of the particles in frictional contact.

VISCOSITY

For the half time step from $\tau = t - \frac{\Delta t}{2}$ to t (i.e., $T = t^-$), the viscous forces depend on the velocity at the end of the half time step. Hence, the viscous forces must be recomputed using the new values of particle velocities at time $\tau + \Delta\tau$. Since the accelerations $(\mathbf{a}_{ex})_{ij}$ are modified if the viscous forces change, the effective frictional accelerations must also be updated. This is achieved using an iterative algorithm (Table IV) in which forces due to the viscosity are added after the frictional forces are applied, and the nonlinear system is subsequently recomputed.

The algorithm shown in Table IV simultaneously iterates the effective friction, particle-pair state, and viscous force, allowing the Newton algorithm for effective friction to converge at the same time that particle-pair state and viscosity are updated.

GLOBAL NUMERICAL INTEGRATION

Table V specifies the global algorithm using the half time step integration scheme. The elastic interactions $(\mathbf{F}_n^I(t^-))$ are first computed using Eq. (6). Once particle accelerations and velocities are updated, viscous forces are incorporated (Table I). The first half time step (from $t - \frac{\Delta t}{2}$ to t^-) ends with the computation of the effective frictional forces (specified by Table IV), where the viscous forces are updated for the particles in frictional interaction. At the second half time step, links are broken for bonded particle-pairs which have a separation r_{ij} greater than r_{break} (links are forced to break at t with $\mathbf{F}_n^I(t^-)$ denoting the elastic force computed before the bond is broken and $\mathbf{F}_n^I(t^+)$, the elastic force after the bond is broken). Frictional accelerations are recomputed and, finally, particle velocities and positions are updated using the modified velocity–Verlat scheme.

TABLE V
Computation of the Two Half Time Steps

First half time step (compute $\dot{\mathbf{x}}_n(t)$ and $\ddot{\mathbf{x}}_n(t^-)$ given $\mathbf{x}_n(t)$ and $\dot{\mathbf{x}}_n(t-\frac{\Delta t}{2})$)

- Update accelerations and velocities:
  - $\ddot{\mathbf{x}}_n^I(t^-) = \frac{1}{M}\mathbf{F}_n^I(t^-)$
  - $\dot{\mathbf{x}}_n(t) = \dot{\mathbf{x}}_n\left(t-\frac{\Delta t}{2}\right) + \frac{\Delta t}{2}\ddot{\mathbf{x}}_n^I(t^-)$
- Incorporate viscous forces for bonded particles (Table I)
- Incorporate frictional and viscous forces for unbonded particles (Table IV)

Second half time step (compute $\dot{\mathbf{x}}_n(t+\frac{\Delta t}{2})$, $\ddot{\mathbf{x}}_n(t^+)$, and $\mathbf{x}_n(t+\Delta t)$ given $\mathbf{x}_n(t)$ and $\dot{\mathbf{x}}_n(t)$)

- Break bonds (compute $\ddot{\mathbf{x}}_n^I(t^+)$ and $\ddot{\mathbf{x}}_n^I(t^-)$)
- Incorporate frictional forces:
  - $\ddot{\mathbf{x}}_n^0(t^+) = \frac{1}{M}\left(\mathbf{F}_n^I(t^+) + \mathbf{F}_n^v(t)\right)$
  - Incorporate frictional forces for unbonded particles (Table III)
  - $\ddot{\mathbf{x}}_n(t^+) = \ddot{\mathbf{x}}_n^0(t^+) + \sum_{l\in P_n}\ddot{\mathbf{x}}_{nl}^F(t^+)$
- Update particle velocities and positions:
  - $\mathbf{x}_n(t+\Delta t) = \mathbf{x}_n(t) + \Delta t\dot{\mathbf{x}}_n(t) + \frac{\Delta t^2}{2}\ddot{\mathbf{x}}_n(t^+)$
  - $\dot{\mathbf{x}}_n\left(t+\frac{\Delta t}{2}\right) = \dot{\mathbf{x}}_n(t) + \frac{\Delta t}{2}\ddot{\mathbf{x}}_n(t^+)$

The precision factor for the numerical integration is given by

$$\epsilon = \frac{V_{\max}\Delta t}{r_0}, \tag{67}$$

where $V_{\max}$ is the maximum velocity in the system, which is approximately equal to 1 (the P-wave speed) if $r_0 = 1$, $k = 1$, and $M = 1$ (Mora and Place [16]). In this case $\epsilon \approx \Delta t$. The choice of ϵ can be used to control the precision of the numerical results. Typically, $\epsilon < 0.2$ must be chosen to obtain results with adequate precision.

ENERGY CONSERVATION

The total energy of the system is computed as the sum of the kinetic energy, potential energy, fracture energy, heat, and applied work done. The conservation of energy provides a check of the numerical integration approach and implementation and is indicative only if the total energy is not constant, in which case an error or imprecision must exist. As was the case for the numerical integration scheme summarised in Table V, the computation of energy by a half time step integration scheme improves the numerical precision.

The kinetic energy, potential energy, and fracture energy (which is the energy lost when a bond is broken) are respectively given by

$$E_{ke}(t) = \sum_{n\in A}\frac{1}{2}M|\dot{\mathbf{x}}_n(t)|^2, \tag{68}$$

$$E_p(t) = \sum_{ij\in I}\frac{1}{4}k(r_{ij}(t) - r_0)^2, \tag{69}$$

and

$$E_f\left(t+\frac{\Delta t}{2}\right) = E_f\left(t-\frac{\Delta t}{2}\right) + \sum_{ij\in B}\frac{1}{4}k(r_{ij}(t) - r_0)^2. \tag{70}$$

The factor is $\frac{1}{4}$ above rather than $\frac{1}{2}$ because the sum is over two interactions: particle i on particle j and particle j on particle i. The kinetic energy lost due to the artificial viscosity (E_ν), computed from

$$E_\nu(t) = -\int_0^t \sum_{n\in A} F_n^\nu \dot{x}_n \, dt, \tag{71}$$

is given by

$$E_\nu(t) = E_\nu\left(t - \frac{\Delta t}{2}\right) + \sum_{n\in A} \frac{\Delta t}{2} \nu |\dot{\mathbf{x}}_n(t)| \left| \dot{\mathbf{x}}_n(t) - \frac{\Delta t}{4} \ddot{\mathbf{x}}_n(t^-) \right|, \tag{72}$$

$$E_\nu\left(t + \frac{\Delta t}{2}\right) = E_\nu(t) + \sum_{n\in A} \frac{\Delta t}{2} \nu |\dot{\mathbf{x}}_n(t)| \left| \dot{\mathbf{x}}_n(t) + \frac{\Delta t}{4} \ddot{\mathbf{x}}_n(t^+) \right|. \tag{73}$$

The total kinetic energy generated is computed as the sum of the kinetic energy (E_{ke}) and the kinetic energy lost due to the artificial viscosity (E_ν) and is given by

$$E_K = E_{ke} + E_\nu. \tag{74}$$

Note that in the above equations, A denotes the set of all particles, I the set of all interacting particle-pairs, and B the set of particle-pairs that have had their bonds broken in the last time step. The work done by the applied intrinsic frictional force (i.e., effective heat) is given by

$$E_h(t) = \int_0^t \sum_{ij\in F} M a_{ij}^F \dot{x}_{ij}^T \, dt, \tag{75}$$

and is computed using

$$E_h\left(t + \frac{\Delta t}{2}\right) = E_h\left(t - \frac{\Delta t}{2}\right) + \frac{M}{2} \sum_{ij\in F} a_{ij}^F(t^-) s_{ij}^-(t) + \frac{M}{2} \sum_{ij\in F} a_{ij}^F(t^+) s_{ij}^+(t), \tag{76}$$

where

$$\begin{aligned} s_{ij}^-(t) &= \Delta t \left(\dot{x}_{ij}^T(t) - \frac{\Delta t}{4} \ddot{x}_{ij}^T(t^-) \right), \\ s_{ij}^+(t) &= \Delta t \left(\dot{x}_{ij}^T(t) + \frac{\Delta t}{4} \ddot{x}_{ij}^T(t^+) \right), \end{aligned} \tag{77}$$

and F denotes the set of interacting particle-pairs. Assuming that heat generated by acoustic vibrations is negligible compared to heat generated by the work done against friction between particles, E_h represents the effective heat generated by the rubbing of particles against each other.

The external work done must also be computed and represents the energy added to the system. For instance, for the numerical experiment described in Fig 6, energy is added to the system in order to move rigid driving plates at a constant rate and to maintain a constant normal stress on the edges. In this case, the external work done is given by

$$W_{ext} = W_{ext}^H + W_{ext}^+ + W_{ext}^-, \tag{78}$$

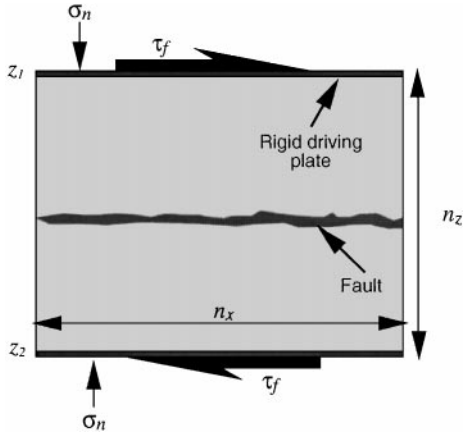

FIG. 6. Illustration of a two-dimensional frictional experiment where the two blocks are composed of $n_x \times n_z$ particles. A normal stress σ_n is maintained in the solid and a shear stress τ_f is applied on the driving plate such that the driving velocity of the edges remains constant.

where W_{ext}^H is the component of external work done to maintain a constant horizontal velocity of the driving plates, and W_{ext}^+ and W_{ext}^- are respectively the work on the upper and lower plates required to maintain a constant normal stress. The work W_{ext}^H done to maintain the constant driving velocities on the plates is

$$W_{ext}^H\left(t+\frac{\Delta t}{2}\right) = W_{ext}^H\left(t-\frac{\Delta t}{2}\right) + \Delta t \sum_{i\in\text{Edges}} (\mathbf{F}_i \cdot \mathbf{e}_x)(\dot{\mathbf{x}}_i(t)\cdot \mathbf{e}_x), \tag{79}$$

where $\mathbf{e}_x$ and $\mathbf{e}_z$ denote the unit vectors in the x and z directions. The external work done on the upper or lower edge to maintain a given constant normal stress σ_n is given by

$$\begin{aligned}
&W_{ext}^+\left(t+\frac{\Delta t}{2}\right)\\
&\quad = W_{ext}^+\left(t-\frac{\Delta t}{2}\right) + \frac{\Delta t}{2}\sum_{i\in\text{Upper edge}} \left(\Delta F_{n_1} + \mathbf{F}_i\cdot\mathbf{e}_z\right)\left[\left(\dot{\mathbf{x}}_i(t) - \frac{\Delta t}{4}\ddot{\mathbf{x}}_i(t^-)\right)\cdot\mathbf{e}_z\right]\\
&\qquad + \frac{\Delta t}{2}\sum_{i\in\text{Upper edge}} \left(\Delta F_{n_1} + \mathbf{F}_i\cdot\mathbf{e}_z\right)\left[\left(\dot{\mathbf{x}}_i(t) + \frac{\Delta t}{4}\ddot{\mathbf{x}}_i(t^+)\right)\cdot\mathbf{e}_z\right],\\
&W_{ext}^-\left(t+\frac{\Delta t}{2}\right)\\
&\quad = W_{ext}^-\left(t-\frac{\Delta t}{2}\right) + \frac{\Delta t}{2}\sum_{i\in\text{Lower edge}} \left(-\Delta F_{n_2} + \mathbf{F}_i\cdot\mathbf{e}_z\right)\left[\left(\dot{\mathbf{x}}_i(t) - \frac{\Delta t}{4}\ddot{\mathbf{x}}_i(t^-)\right)\cdot\mathbf{e}_z\right]\\
&\qquad + \frac{\Delta t}{2}\sum_{i\in\text{Lower edge}} \left(-\Delta F_{n_2} + \mathbf{F}_i\cdot\mathbf{e}_z\right)\left[\left(\dot{\mathbf{x}}_i(t) + \frac{\Delta t}{4}\ddot{\mathbf{x}}_i(t^+)\right)\cdot\mathbf{e}_z\right],
\end{aligned} \tag{80}$$

where

$$\Delta F_{n_1} = \Delta F_{n_2} = F_n - \frac{1}{2}\left(\bar{\mathbf{F}}_{z_1} - \bar{\mathbf{F}}_{z_2}\right)\cdot\mathbf{e}_z, \tag{81}$$

or

$$\Delta F_{n_i} = F_n - \bar{\mathbf{F}}_{z_i} \cdot \mathbf{e}_z, \tag{82}$$

for the upper and lower edges ($i = 1$ and $i = 2$, respectively). In the above equations F_n denotes the normal force corresponding to a normal stress σ_n. Equations (81) and (82) decribe different ways to maintain a contant pressure. In Eq. (81) the same normal force is applied on the lower and upper edges whereas in Eq. (82) the two edges are independent, which is more appropriate for simulating normal stress in the brittle crust.

In Eq. (80), $\Delta F_{n_i} + \mathbf{F}_i \cdot \mathbf{e}_z$ represents the normal force applied to the upper or lower edge ($i = 1$ or $i = 2$, respectively), n_x is the number of particles along the edge, and $\bar{\mathbf{F}}_{z_i}$ is the average value of the force on one particle for a row of particles at $z = z_i$ (z_1 for the upper edge and z_2 for the lower edge, as shown in Fig. 6),

$$\bar{\mathbf{F}}_{z_i} = \frac{1}{n_x} \sum_{j=1}^{n_x} \mathbf{F}_{(j,z_i)}, \tag{83}$$

where $\mathbf{F}_{(j,z_i)}$ is the total force acting on the particle located at row z_i and column j.

F_n in model units is assumed to produce the same strain in the elastic model as a normal stress of σ_n in pascal units in a medium having typical values of elastic constants for the crust (i.e., corresponding to a compressional wave speed $V_p = 3\sqrt{3}$ km/s and a density of the medium $\rho = 3000$ kg/m^3).

UNIT CONVERSION

Scaling between systems of units is required in order to compare results obtained with the model in arbitrary model units with real data or laboratory observations. In the following we consider two unit systems: MKS units denoted by prime ($'$) and the model units (no prime). The normal force arising from a relative normal displacement of u is $F_n = ku$, where k is the spring constant (or the stiffness between two particles). Hence,

$$\frac{F_n'}{F_n} = \frac{k'u'}{ku}. \tag{84}$$

Since strains (ϵ_n) are proportional to displacements divided by distance r_0, we have

$$\frac{F_n'}{F_n} = \frac{k'\epsilon_{n'}r_0'}{k\epsilon_n r_0}. \tag{85}$$

The strains in the model equal the strains in the real system, so $\epsilon_n = \epsilon_{n'}$, which leads to

$$F_n = \frac{F_n' k r_0}{k' r_0'}. \tag{86}$$

In the 2D lattice solid, the stress in the MKS units system ($\sigma_{z'z'}$) is given by

$$\sigma_{z'z'} = \frac{F_n'}{r_0'}, \tag{87}$$

where r_0' is the particle diameter. Using Eqs. (86) and (87) we obtain

$$F_n = \sigma_{z'z'} \frac{k}{k'} r_0. \tag{88}$$

If we set $k = 1$ in model units, and assuming that we wish to use MKS units to specify the normal stress σ_n and k' (i.e., F_n in Pascals) are in MKS units, Eq. (88) becomes

$$F_n = \frac{\sigma_n}{k'} r_0, \tag{89}$$

where k' can be deduced from

$$\lambda = \mu = k' \frac{\sqrt{3}}{4}, \tag{90}$$

which is given in Mora and Place [16]. Namely, if we make use of $V_p = \sqrt{\frac{\lambda+2\mu}{\rho}}$, Eq. (90) yields

$$k' = \frac{\lambda + 2\mu}{3} \frac{4}{\sqrt{3}} = \rho V_p^2 \frac{4}{3\sqrt{3}} = \frac{4\sqrt{3}}{9} \rho V_p^2. \tag{91}$$

Consequently, to maintain a normal stress σ_n in Pascals, the normal force F_n in model units that must be applied is

$$F_n = \frac{9}{4\sqrt{3}} \frac{\sigma_n}{\rho V_p^2} r_0. \tag{92}$$

TOTAL ENERGY AND HEAT ERROR TERM

The normalised total energy, given by

$$E(t) = \frac{E_K(t) + E_p(t) + E_f(t) + E_h(t) + W_{ext}(t)}{E_K(t_0) + E_p(t_0) + E_f(t_0) + E_h(t_0) + W_{ext}(t_0)}, \tag{93}$$

is computed. This value should remain close to unity if the scheme is accurate. The conservation of energy is not indicative of the validity of the results, but failure to conserve energy would indicate a problem in the numerical approach. For example, as the time step is increased, the numerical energy varies substantially with time due to increasing inaccuracy of the finite difference scheme in representing the time derivative. Similarly, failure to model friction precisely during the numerical integration procedure results in time variation in the computed numerical energy.

The computation of heat using Eq. (76) allows "negative heat" to be generated if the tangential velocity $\dot{\mathbf{x}}_{ij}^T$ changes sign during a half time step (i.e., bouncing pairs). If the simple iterative approach described previously is used, a negative value for heat means that the frictional forces are not correct. In the Cundall approach to computing friction, the work done by intrinsic friction also includes energy absorbed or restored in the shear deformation of the particles. Hence, "negative heat" is not indicative of a fundamental error within the method (i.e., it is self-consistent). However, negative heat generation can indicate an error in dynamics relative to the desired result: when two particles are locked by static friction,

part of the energy is stored as shear deformation of the particle. If the frictional forces are underestimated or overestimated, the particle will restore or release some of the energy stored in shear deformation. This results in tangential oscillation of the particle around the point of contact. An excessive "negative" heat generation (typically, the energy released from the particle shear deformation is one order of magnitude less than the total work done by intrinsic friction using a shear stiffness, $k_s = k$) would indicate that particles are unphysically oscillating due to incorrect frictional forces. These oscillations can also cause non-physical changes in frictional behaviour (i.e., changing between static and dynamic frictional behaviour).

However, a positive value for heat may or may not be correct. For example, if the tangential velocity changes in sign (i.e., bouncing particle), a positive value of heat may be incorrect (the frictional force may oppose the direction of slip at the end of the time step but will not oppose the direction of slip during the entire time step since the slip is reversing during the time step).

By summing the "negative heat" generated (E_h^-), a lower bond of the component of the energy restored to the system by applying a frictional force which is too large or too small can be evaluated:

$$\varepsilon_h = \left| \frac{E_h^-}{E_h - E_h^-} \right|. \tag{94}$$

In the lattice solid model, the work done by intrinsic friction (i.e., effective heat) for bouncing particle-pairs can have a negative value while the correct dynamics is simulated. In order to compute the "true" or effective heat generated during a simulation, the effective heat for bouncing particles is computed using Eq. (76), where the effective frictional forces a_{ij}^F are set to the true value of the frictional acceleration (i.e., a_{ij}^F is respectively equal to $\hat{\mathbf{a}}_{ij}^F(T)$ and $\hat{\mathbf{a}}_{ij}^F(T + \Delta\tau')$ before and after the tangential velocity passes through zero). Consequently, for the lattice solid approach, the negative heat measured by Eq. (94) is an overestimate of the error. With the lattice solid approach, the negative heat generated by friction between all particles, except bouncing particle-pairs, is typically 5 orders of magnitude less than E_h^-. Hence E_h^- for the lattice solid approach represents mainly the "negative" heat generated by bouncing particle pairs. Since bouncing particle-pairs can produce "negative" heat while simulating the desired dynamics, ε_h potentially overestimates the error in the lattice solid approach by up to several orders of magnitude.

LIMITATIONS AND FUTURE WORK

Particles in the model represent idealized grains or units of rock. This representation has limitations, in that particles do not rotate and do not have moments of inertia. Furthermore frictional forces are applied at the particle centres and not at the particle surfaces. To overcome these limitations, particles can be used as the building blocks of grains or, alternatively, rotation at the particle scale can be included and friction applied at particle surfaces as in Winter *et al*. [25]. By grouping particles to form unbreakable model grains of rock, rotation can be simulated and frictional forces applied at the grain surface in the limit of large multi-particle grains. While single particles effectively have infinite shear stiffness, grains can be deformed when subjected to shear stress. Because grains in the model are the smallest indivisible unit of the system, unlike those in real rocks, they cannot break to

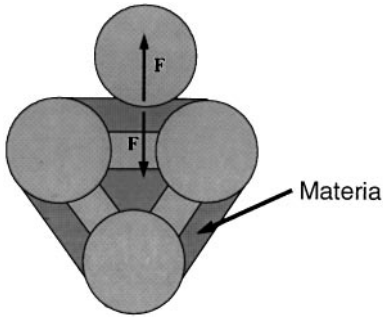

FIG. 7. Concept of modeling the interactions between particles and bonds. The space between bonded particles is filled by material and interacts accordingly with other particles.

form smaller grains of rock. In the following examples, grains are composed of only 3 to 10 particles due to computer limitations. Consequently grains have a high surface roughness. To specify a realistic surface roughness, a possible solution would be to fill the spaces between bonded particles with material and to allow interactions between fill material and particles to be modelled (Fig. 7). The use of particles of different sizes would also allow more realistic surface roughness to be specified, and would reduce the porosity to a more realistic value (cf. a rock with non-uni-modal grain size). This solution would also enable random lattices to be specified, and hence, isotropic fracture behavior could be modelled. By using particles of different sizes and filling the space between bonded particles, grain shapes and fault surface roughness could be more precisely controlled, thus enabling more realistic geometries to be modelled.

The heat generated during a simulation is defined as the work done by intrinsic friction between particles. Because attenuation of acoustic vibrations is not modelled, the calculation of heat does not take into account heat that would in reality eventually be generated by acoustic vibrations.

RESULTS

The purpose of the first set of numerical experiments is to show that results obtained with the model are consistent with our theoretical expectation and with field observations. These tests consist of (1) verifying that the heat generated during earthquakes (defined as the work done against microscopic intrinsic friction) is in accordance with a simple theoretical prediction (work done at the macroscopic scale); (2) verifying that the stick–slip frictional behaviour is observed and is similar to other observations.

The purpose of the following numerical experiments is to check the numerical precision and the validity of the results when an intrinsic friction is specified by verifying that the heat produced during microscopic slips between particles is the same as a value that would be theoretically expected from macroscopic slip between the fault surfaces, assuming that a coefficient of friction is equal to the particle intrinsic friction. The normalised total energy given by Eq. (93) is plotted to verify the precision of the numerical approach.

The numerical experiment (Fig. 8) consists of two homogeneous elastic blocks where the surfaces are essentially flat to within the resolution of the model (i.e., surface height variation $h_s = (1 - \frac{\sqrt{3}}{2})r_0$). Circular conditions are applied along the x axis. The blocks, composed of 64×32 particles, are pushed past one another by moving the rigid driving plates at a

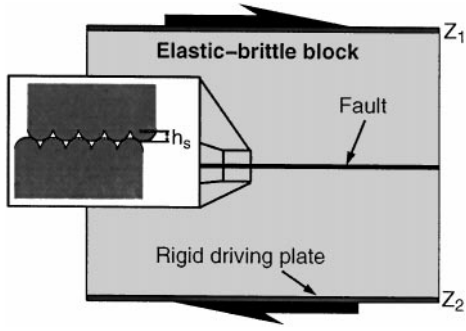

FIG. 8. Two-dimensional experiment involving two elastic blocks composed of 64×32 particles, where a constant normal stress of 300 MPa is maintained on the rigid driving plates and a frictional coefficient of $\mu = 0.8$ is used. The block surfaces are flat to within the limits of the discretisation (i.e., the roughness is not zero because the smoothest surface that can be defined using the lattice solid model is a row of particles).

constant rate of $\sim 0.00024 V_p$ (where $V_p = \sqrt{\frac{9}{8}}$ using $k = 1$ and $M = 1$), while maintaining a given normal stress σ_n on the rigid driving plates. A "normal stress" of 300 MPa was used in this numerical experiment, which approximately corresponds to the upper limit of the normal stress at middepth in the brittle crust. The viscosity of the medium is set to $\nu = 0.064$. The normal stress is computed using a compressional wave speed of $V_p = 3\sqrt{3}$ km/s and a density $\rho = 3000$ kg/m^3 (cf. Eq. (89)). The breaking separation (r_{break}) is set to $1.1 r_0$, which can be considered the upper limit for most materials (Mora and Place [16]). Figure 9 shows the observed macroscopic coefficient of friction of the model fault defined as the ratio of shear to normal stress given by

$$\mu_f(t) = \frac{\tau_f(t)}{\sigma_n(t)} = \frac{\left(\bar{\mathbf{F}}_{z_1}(t) - \bar{\mathbf{F}}_{z_2}(t)\right) \cdot \mathbf{e}_x}{\left(\mathbf{F}_{z_1}(t) - \mathbf{F}_{z_2}(t)\right) \cdot \mathbf{e}_z}, \tag{95}$$

where τ_f is the shear stress measured on the driving plates, and σ_n is the normal stress. $\bar{\mathbf{F}}_{z_i}$ is the average value of the force for a row of particles at $z = z_i$ (z_1 for the upper edge and z_2 for the lower edge of the lattice). Assuming that energy goes mainly into seismic

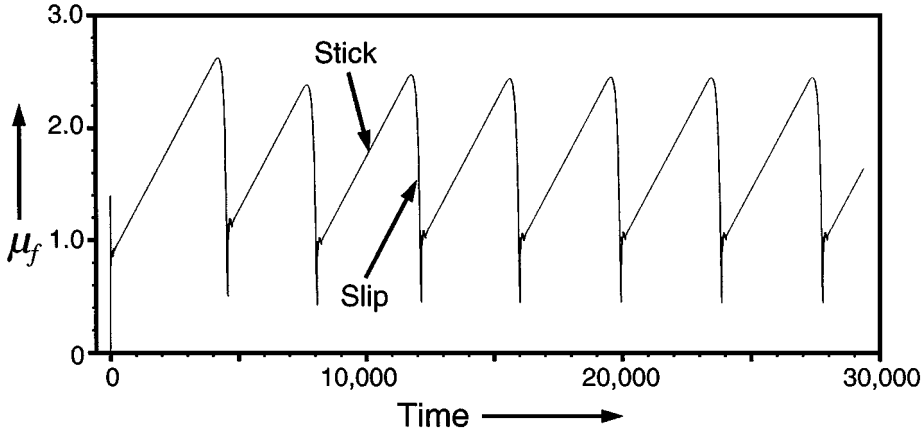

FIG. 9. Plot of the observed coefficient of friction measured on the rigid driving plates showing stick–slip cycles.

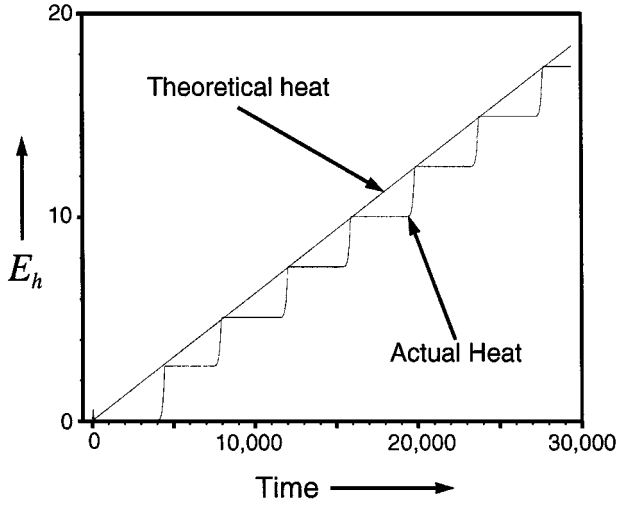

FIG. 10. Heat generated using the lattice solid model approach in an example in which the numerical error in heat remains less than 0.01% and the heat generated is equal to the theoretical value. The staircase appearance of the actual heat is due to the stick–slip movement of the fault.

waves and heat (this is a true assumption, considering the fact that during the experiment no fracturing occurred and there are no transformations of energy other than kinetic and heat), the frictional stress on the fault, τ_f, can be expressed as the sum of the frictional stress going into seismic waves (due to surface roughness) and heat (due to intrinsic friction between particles). Hence, the observed coefficient of friction represents the sum of the surface roughness effect and intrinsic friction between particles. Stick–slip cycles can be seen as the characteristic sawtooth shape observed in laboratory experiments.

Figure 10 shows the "actual heat" (i.e., heat generated when particles rub past one another) and the "theoretical heat" given by

$$E_{th}\left(t+\frac{\Delta t}{2}\right)=E_{th}\left(t-\frac{\Delta t}{2}\right)+2V\Delta t\frac{\mu}{r_0}\left[\left(\bar{\mathbf{F}}_{z_1}(t)-\bar{\mathbf{F}}_{z_2}(t)\right)\cdot\mathbf{e}_z\right], \tag{96}$$

where V is the driving plate velocity. The theoretical heat represents the heat that would be generated by rubbing two blocks of rock past one another at a constant velocity V, where the coefficient of friction of the rock is μ ($E_{th}=\mu\sigma_n 2LVt$, where L is the length of the driving plates). In this numerical experiment, the heat generated follows the same trend as that of the theoretical value, and the error in heat (given by Eq. (94)) remains less than 0.01%.

The purpose of the next two sets of numerical experiments is to verify that the friction of the model fault is equal to the theoretical value for different sets of parameters.

In the first set of numerical experiments, the normal stress was constant (300 MPa) and the frictional coefficient μ was varied from 0.1 to 0.9. The effective macroscopic coefficient of friction (producing heat) is given by

$$\bar{\mu}_h=\mu\frac{\bar{E}'_h}{E'_{th}}, \tag{97}$$

where $\bar{E}'_h$ and $\bar{E}'_{th}$ are respectively the average rate of heat actually generated (computed as the work done against intrinsic friction) and heat theoretically generated (given by Eq. (96)).

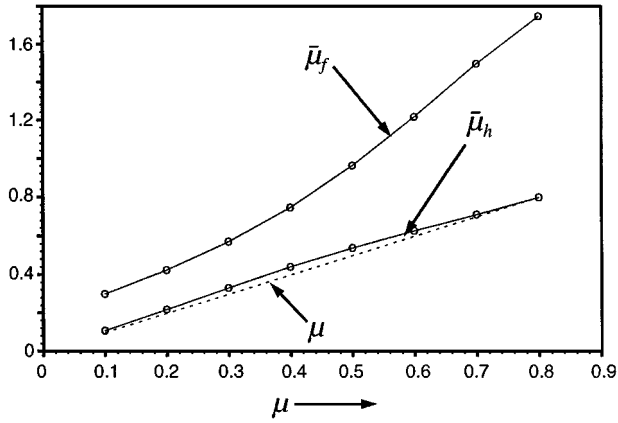

FIG. 11. Observed macroscopic coefficient of friction and effective macroscopic coefficient of friction compared to the theoretical value μ (dashed line). The minimum observed macroscopic coefficient of friction is not zero because the fault roughness is not zero.

The ratio between these two values should be close to unity if the heat generated remains close to the theoretical value. In this case, the effective macroscopic coefficient of friction should be equal to the microscopic coefficient of friction μ. Figure 11 shows the observed macroscopic coefficient of friction ($\bar{\mu}_f$) computed as the average value of μ_f (Eq. (95)) and the effective macroscopic coefficient of friction, $\bar{\mu}_h$ as a function of μ. In these numerical experiments, the effective coefficient of friction remains approximately equal to the microscopic coefficient of friction μ, the total energy is constant to within an error of 0.1%, and the error in heat is less than 0.01%.

In the second set of numerical experiments a frictional coefficient μ equal to 0.8 and a normal stress σ_n ranging from 25 to 400 MPa are used. Figure 12 shows the observed macroscopic coefficient of friction ($\bar{\mu}_f$) and the effective macroscopic coefficient of friction ($\bar{\mu}_h$), which would theoretically be expected to equal the microscopic coefficient of friction μ.

For pressure greater than $\sim$250 MPa, the effective macroscopic coefficient of friction $\bar{\mu}_h$ in Figs. 11 and 12 follows the expected value. However, in Fig. 12 the observed coefficient

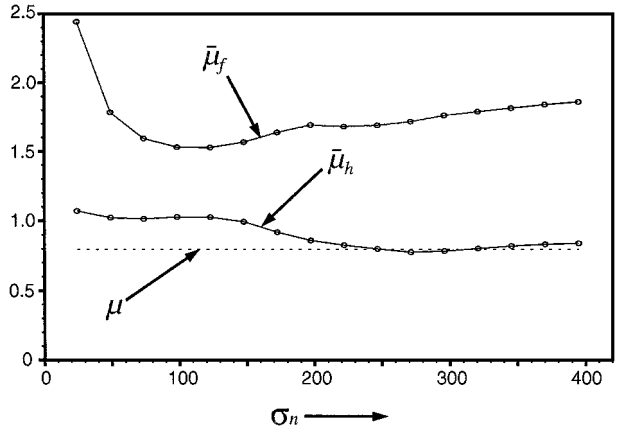

FIG. 12. Observed macroscopic coefficient of friction and effective macroscopic coefficient of friction compared to the theoretical value μ (dashed line) as a function of the normal stress.

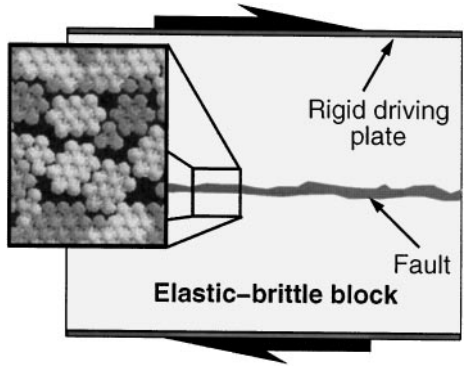

FIG. 13. Example of a setup for a numerical friction experiment. The two blocks are pushed by moving the driving plates at a constant rate. The lattice is made of grains composed of 3 to 10 particles.

of friction tends to be higher than the theoretical prediction, especially at low values of the normal stress. This is essentially due to a dynamical effect enhanced by the low normal pressure and the regularity of the surface roughness where the slip can eventually reverse (overshoot effect leading to slip that is more than a simple sliding movement of surfaces, and thus, to more heat generated).

NUMERICAL EXPERIMENT

The two-dimensional numerical friction experiment (Fig. 13) consists of two homogenous elastic blocks separated by a gouge layer. The lattice is composed of 128×128 particles. Two regions can be distinguished: the gouge region and the elastic region (outside the gouge region). The elastic region is unbreakable and hence represents a pure elastic material. The gouge region is composed of grains which are not bonded mutually. Grains themselves are composed of 3 to 10 particles which are bonded by strong links (i.e., $r_{break} = 1.5r_0$). The distribution of grain sizes in the gouge region is inversly proportional to the grain sizes. Normal stress is maintained at 150 MPa on the driving plates while the plates are pushed at a constant velocity of $\sim 0.00024 V_p$, where V_p represents the P-wave velocity ($V_p = \sqrt{\frac{9}{8}} \sim 1.0$ for a spring constant $k = 1$ and a particle mass $M = 1$; see also Mora and Place [16]).

STICK–SLIP INSTABILITY

The observed coefficient of friction during the friction experiment, computed using Eq. (95), shows the characteristic sawtooth shapes of stick–slip frictional behaviour (Fig. 14) and a complex distribution of event sizes. The numerical experiment involves a system of 128×128 particles. The lattice is made of grains composed of 3 to 10 particles, where the grain distribution is homogeneous. The coefficient of friction $\mu = 0.42$, $r_{break} = 1.5r_0$ inside a grain, and $r_{break} = 1.04r_0$ between grains, and a constant normal pressure $\sigma_n = 150$ MPa is maintaned at the driving plates.

FAULT GOUGE AND HEAT OF EARTHQUAKES

A long-standing paradox in earthquake studies has been the heat flow paradox (Lachenbruch and McGarr [9], Lachenburg and Sass [10]), namely, that the heat flow

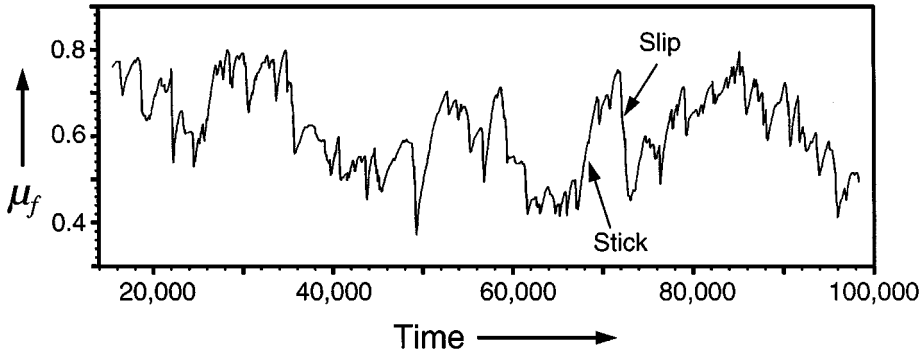

FIG. 14. Observed coefficient of friction during a frictional experiment showing stick–slip cycles.

observed along the San Andreas fault is at least five times less than the theoretically predicted value. With different values of the intrinsic friction from 0.1 to 3.2 and a setup similar to that specified previously, simulations show that the actual heat due to rubbing between particles (Eq. (76)) is up to 10 times less than the theoretical value (Fig. 15). (See also Mora and Place [18, 19] for a comprehensive presentation of these and related results which provide a possible explanation of the heat flow paradox and associated observations.)

During the simulation, slip pulses are sometimes observed that propagate along the fault in a manner similar to that observed by Brune and co-workers [3] in stick–slip experiments on foam rubber. However, analysis of the results (Mora and Place [18, 19]) show that a reduction in normal stress between grain surfaces during slip cannot explain the low heat observed. This suggests that neither the Brune-type local reduction in normal stress (coherent with a slip pulse) nor the Melosh-type incoherent reduction in normal stress ("acoustic-fluidisation" model; Melosh [13]), if present, is the dominant cause of heat reduction in the numerical experiments. Rather, the analysis of Mora and Place [18, 19] showed that the low value of heat is explained by rotation of grains (jostling and rolling) with minimal slip of grain surfaces during slip of the fault, a mechanism which is promoted by the high value of the intrinsic friction (or rounder grains).

This "clean rotation" reduces the amount of slip between surface particles of grains and consequently reduces the heat generated during a macroscopic slip event of the model fault. Numerical experiments show that when grains are allowed to break down to one particle

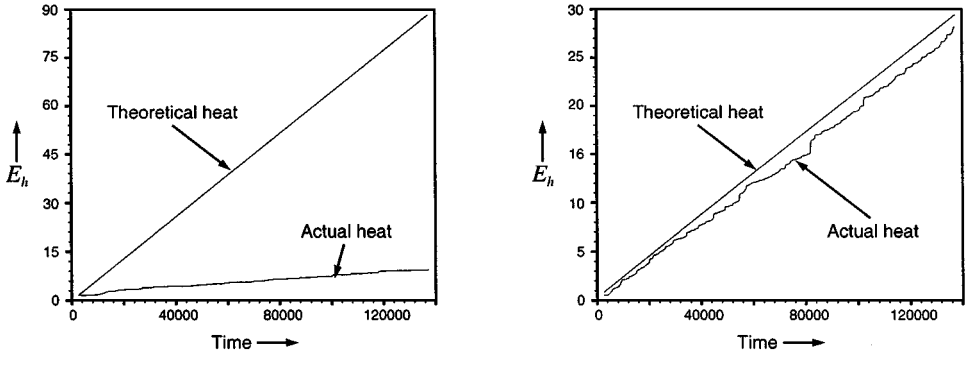

FIG. 15. Actual heat compared to theoretical predictions when (left) a high value of intrinsic friction is used (i.e., $\mu = 1.7$), and when (right) a low value of intrinsic friction is used (i.e., $\mu = 0.42$).

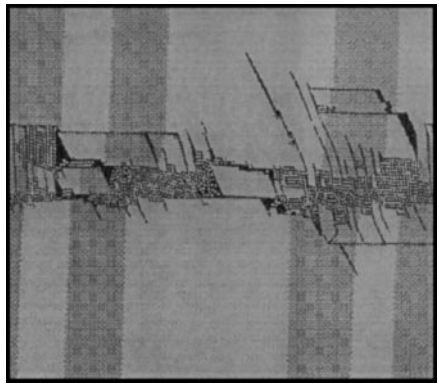

FIG. 16. Snapshots of simulations in which fault gouge was generated.

only (irrotational units that only allow slip), a fault develops that is mainly composed of free particles (Fig. 16). The lattice is composed of 128×128 particles which are the smallest indivisible units of the system. The value of r_{break} is uniformly equal to $1.05r_0$ and $\mu = 0.85$. When a slip event occurs, free particles slip against one another (free particles are unable to rotate since rotation is not modelled in the current version of the lattice solid model). Hence, more heat is generated when grains do not rotate than when rotation of grains is allowed, but still less than the theoretical value in some instances (up to 50% less). This is due to a physical bouncing mechanism (similar mechanisms are known to reduce friction and have been studied previously in Pisarenko and Mora [20]) that allows particles to slip past one another while the normal stress is temporally reduced. This result suggests that while rolling is the dominant low heat mechanism in the numerical experiment, bouncing-type mechanisms may superimpose on this effect in a simulation using grouping of particles. This is verified by detailed calculation in Place and Mora [24].

COMPUTATIONAL NEEDS

The system size for simulations was 128×128 or 256×256 particles and is too small to specify realistic fault systems or rock surface roughness. Computations involving intrinsic friction are highly time consuming when fault gouge develops because the nonlinear system which must be solved to compute the static frictional acceleration is proportional to the number of touching particles (Eq. (49)). Therefore, efficient algorithms are required to reduce the computational time.

A typical simulation involving two blocks of 128×64 particles requires approximately 250,000 units of time (with $k = 1$ and $M = 1$). In other words, if the time step increment Δt is 0.04 (for a precise numerical solution with intrinsic friction), the simulation will require 50 million time steps (approximately two months of computation on a 1.2 GFlops computer).

In order to reduce the number of time steps required for a simulation, the time step increment Δt must be as large as possible for the required precision to be obtained. The precision factor (given by Eq. (67)) relates to the maximum velocity and the time step increment where a large time step increment can be used when particle velocities are small (a time step increment of 0.2 is required to obtain results with adequate precision, assuming that the maximum velocity is approximately equal to 1, the P-wave speed, if

$r_0 = 1$, $k = 1$, and $M = 1$). A time step increment of 0.4 may be sufficient for a stable and accurate numerical integration in much of the run such as during static stress buildup phases. However, a time step increment of 0.04 is typically required to capture discontinuities due to frictional interactions, precisely compute the frictional forces, and yield an accurate numerical integration when the system is undergoing a dramatic dynamical event (such as a simulated earthquake). An adaptive time step increment has therefore been developed that enables a large time step increment to be used during periods of quiescence of the simulation (i.e., stick phase). The time step increment is chosen as a function of the maximum particle velocity using

$$\Delta t(t) = \begin{cases} \max(\Delta t_\gamma(t), \Delta t_{\min}), & |\dot{\mathbf{x}}|_{\max}(t) > K \\ \Delta t_{\max}, & |\dot{\mathbf{x}}|_{\max}(t) \le K, \end{cases} \tag{98}$$

where

$$\Delta t_\gamma(t) = \Delta t_0 \frac{(1-\gamma)K'}{|\dot{\mathbf{x}}|_{\max}(t)} + \gamma \Delta t_\gamma(t - \Delta t), \tag{99}$$

$$\gamma = \begin{cases} \gamma_1, & \text{if } |\dot{\mathbf{x}}|_{\max}(t) \ge |\dot{\mathbf{x}}|_{\max}(t - \Delta t) \\ \gamma_2, & \text{otherwise.} \end{cases} \tag{100}$$

The maximum particle velocity is denoted by $|\dot{\mathbf{x}}|_{\max}$ and Δt_0 represents the normal time step increment ($\Delta t_0 = 0.2$) that is suitable for wave propagation and "non-violent" dynamic events. The maximum time step increment $\Delta t_{\max}$ (typically, $\Delta t_{\max} = 0.5$) is the largest time step that is suitable for numerical stability and that can be used where no dynamic event is occurring. The minimum time step increment $\Delta t_{\min}$ is the largest time step that can be used when a "violent" dynamic event occurs (typically $\Delta t_{\min} = 0.04$). The constant K is an average of particle velocity and represents the minimum particle velocity when no dynamic events are occurring. The constant K' is used to scale the time step increment and γ is used to control the rate of change of the time step increment. K' and γ are chosen such that a large time step increment will be used when no simulated earthquake events are occurring (i.e., stick phase), and will quickly decrease when a simulated earthquake is initiated in order to capture changes in frictional behaviour. To capture events triggered by other events the time step should also increase slowly once all radiated energy (seismic waves) from an earthquake has been dissipated.

For example, for small particle velocity (i.e., $|\dot{\mathbf{x}}|_{\max}(t) < K'$) the time step will approach Δt_0. The value of K' is typically chosen as the typical particle velocity when waves propagate in the solid but no "violent" dynamic event is occurring. A small value of γ_1 is chosen to allow the time step increment to rapidly adapt when the particle velocities are increasing during initiation of a slip phase, for instance (typically, $\gamma_1 = 0.1$ to rapidly capture stick–slip instabilities). A large value of γ_2 will ensure a gradual increase of the time step increment when the particle velocities are decreasing (typically, $\gamma_2 = 0.9$ to capture aftershocks or main shocks occurring after precursory events). The time step increment is recomputed after each half time step (specified in Table V) at the middle and at the end of a time step. If at the end of a time step, the calculated time step increment decreases, that is, a value that was too large was used during the last half time step, then the time step is halved and recomputed using the newly computed time step.

Typically, a variable time step leads to a reduction of approximately 300% in the number of time steps compared to a simulation using a constant time step increment of 0.04.

The solution of the linear system (Eq. (55)) to compute frictional forces is also optimized. The linear system involves a square matrix $\nabla \mathbf{q}$ of all interacting particle-pairs. A simulation involving 128×128 particles may typically have up to 2000 interacting particle-pairs, so the size of the matrix $\nabla \mathbf{q}$ will be 2000×2000. Since all elements of the matrix $\nabla \mathbf{q}$ are zero except for particle-pairs which interact with one another, only the non-zero elements are stored in memory. This sparse system is solved using an LDU decomposition.

A reduction in computational needs is critical for large scale simulations, where the model size is limited by the computational time required to compute the frictional forces. Unfortunately, model sizes used (128×128 and 256×256) were insufficient to specify realistic rock surface roughness (e.g., as observed and described by Brown and Scholz [4]) or fault systems. Up to 40% of the time (when a large fault gouge develops) is spent solving the linear system to compute the frictional acceleration (even using a highly optimized sparse LU solver). Hence the efficiency of the program as a whole depends mostly on the efficiency of the algorithm in solving a "sparse" linear system (see also Place and Mora [23]).

CONCLUSIONS AND PERSPECTIVES

Incorporation of intrinsic friction into the lattice solid model enables more realistic and accurate simulations of the physics of rocks and the dynamics of earthquakes to be performed using the lattice solid model.

This is achieved by specifying interactions between model particles in a such way that no slip is observed between particles when two surfaces are locked by static friction. The numerical approach is based on a half time step interaction scheme in which the discontinuity due to bond breaking is precisely captured. Transition between static and dynamic frictional behaviour is modelled by introducing intermediate states for particle-pairs undergoing this transition or bouncing against one another. Static frictional forces are computed by resolving a nonlinear system involving all frictional interactions that effectively lock grains at the contact point (stop slip between surface particles of grains).

The lattice solid model provides a precise, reliable, and efficient approach which can be used to quantitatively study heat generation and problems of geophysical significance such as the heat flow paradox. Such studies have already provided a comprehensive possible explanation for this geophysical paradox. By simulating microscopic frictional instabilities (the transition between static and dynamic behavior), the model is able to simulate complex phenomena occurring in large nonlinear dynamical systems, such as precursory phenomena which may occur before a large earthquake. Future studies of such phenomena may provide clues to the predictability of earthquakes.

APPENDIX: COMPARISON OF DIFFERENT NUMERICAL APPROACHES

The numerical experiment (Fig. 17) consists of two homogeneous elastic blocks where a constant normal stress of 1470 MPa (using $V_p = 3\sqrt{3}$ km/s and $\rho = 3000$ kg/m^3) is maintained on the edges of the lattice and a frictional coefficient $\mu = 0.8$ is used. The block surfaces are flat to within the model discretisation.

Several simulations are performed using three different methods: the interative method (the first simple approach proposed), the Cundall approach applied to the lattice solid model, and the current lattice solid model approach. The joint stiffness K_s used for Cundall's approach is set to 1.0.

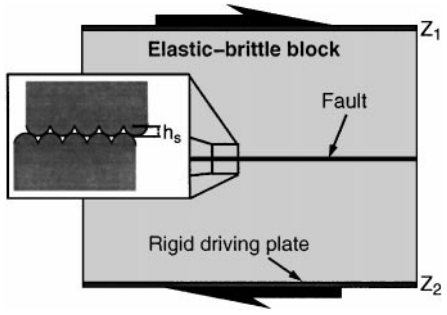

FIG. 17. Two-dimensional experiment involving two elastic blocks composed of 64 × 32 particles. The block surfaces are flat to within the limits of the discretisation (i.e., the roughness is not zero because the smoothest surface that can be defined using the present lattice solid model is a row of particles).

Figure 18 shows the observed coefficients of friction for the three methods using the same set of parameters. The observed coefficient of friction μ_f is given by

$$\mu_f(t) = \frac{\tau_f(t)}{\sigma_n(t)} = \frac{\left(\bar{\mathbf{F}}_{z_1}(t) - \bar{\mathbf{F}}_{z_2}(t)\right) \cdot \mathbf{e}_x}{\left(\mathbf{F}_{z_1}(t) - \mathbf{F}_{z_2}(t)\right) \cdot \mathbf{e}_z}, \tag{A.1}$$

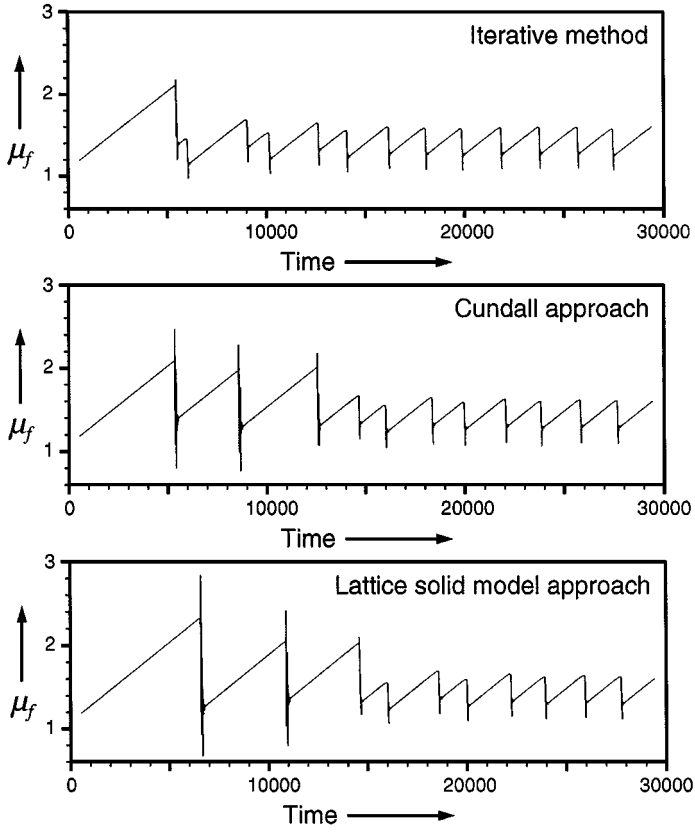

FIG. 18. Observed coefficient of friction using the iterative method (top), the Cundall approach (middle), and the lattice solid model approach (bottom). Stick-slip cycles became more regular after the initial events. These initial events are different for each method, with slip seeming to occur more easily for the two first methods.

where τ_f is the shear stress measured on the driving plates, σ_n is the normal stress, and $\bar{\mathbf{F}}_{z_i}$ is given by Eq. (83).

The time step increment is allowed to range from 0.1 to 0.2 except in the Cundall approach, where a fixed time step increment of 0.1 is used in accordance with Eq. (38). Note that from Eq. (38), a value of Δt small enough that $\Delta\tau = \frac{\Delta t}{2} < 0.14$ must be chosen. However, a value of $\Delta t = 0.1$ was found to be small enough to ensure numerical stability, considering the fact that the user-defined factor c in Eq. (38) relates to the number of simultaneous contacts that a particle can have. Since a particle interacts with a maximum of two unbonded particles in this numerical experiment, one can use a value for c greater than that possible in 3D simulations ($c \approx 0.2$ in this case).

The plot of the maximum particle velocity during a slip event using the iterative method (Fig. 19) highlights an instability which may occur before a slip. This instability is due to oscillation of particles between static and dynamic frictional behaviour before a slip.

In all three methods, the total energy remains constant to within 1% during the simulation. Total energy alone cannot be used to check the physical validity of the numerical approach, considering, for example, the fact that energy added due to a wrong value of frictional forces

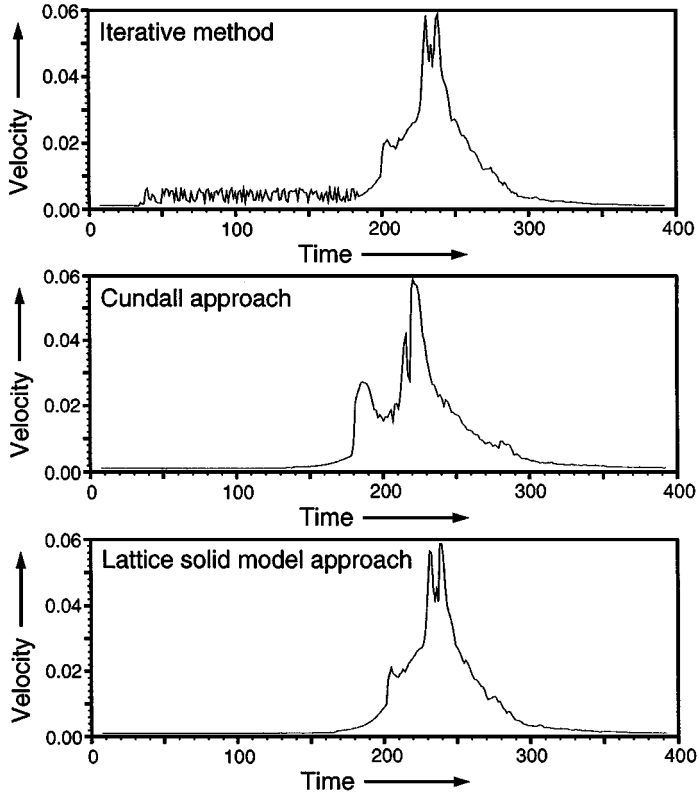

FIG. 19. Maximum particle velocity using the iterative method (top), the Cundall approach (middle), and the lattice solid model approach (bottom). A numerical instability appears when the first method is used due to particles oscillating between static and dynamic frictional behaviour. The dynamic behaviour in the Cundall approach seems to be different from that of the other two methods. This is presumably because particles in static frictional contact in these methods are seen as having high shear stiffness whereas the use of $K_s = 1$ in Cundall's method effectively introduces a shear stiffness at the particle scale.

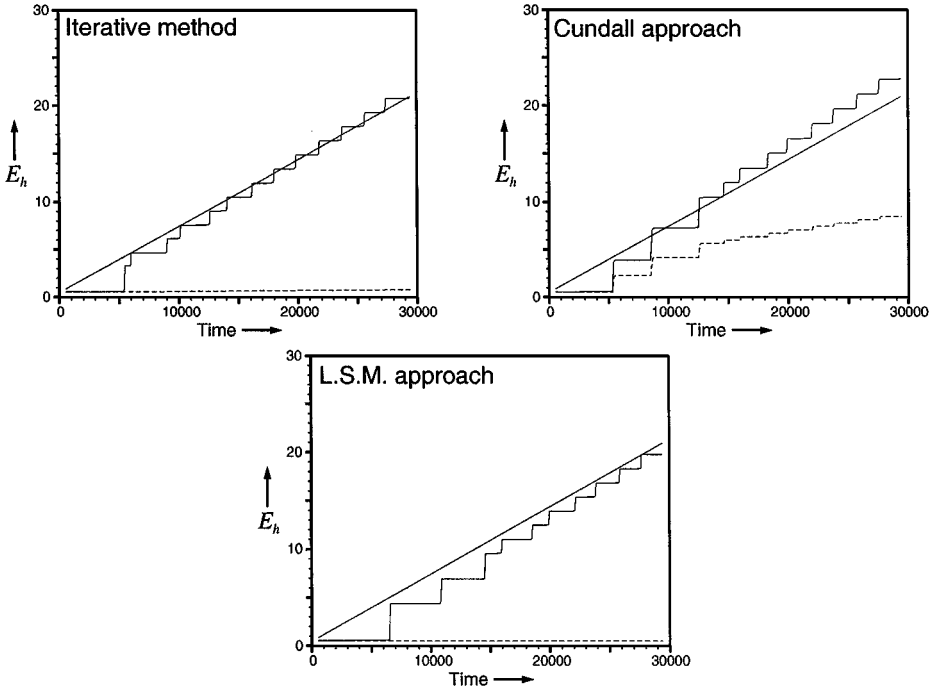

FIG. 20. Heat generated (fine solid line) compared to the theoretical value (bold solid line) using the iterative method (top left), the Cundall approach (top right), and the lattice solid model approach (bottom). The numerical error in the heat generated (dashed line) is magnified by a factor of 2. The theoretical value is computed as the work done to move the driving plates, assuming that the horizontal stress on the plates is $\tau_f = \mu\sigma_n$.

will not be detected (i.e., a wrong heat is balanced by an error in kinetic energy). However, the heat energy should always be positive for the iterative approach and the lattice solid model, so any negative heat in the calculations provides a measure of the physical validity (that is, the frictional force must oppose the direction of slip). For the Cundall approach, this term relates to the energy restored by the particle shear stiffness and is indicative of an error only if this term is excessively high. Such a measure is termed the numerical error ε_h in the heat and is computed using Eq. (94).

Figure 20 shows the actual heat, the theoretical heat, and the numerical error in heat. The Cundall approach shows an error in the heat of 20%, which is essentially due to use of a finite joint stiffness K_s and represents the energy absorbed or restored by the particle shear elasticity when the contact is static.

Even though the iterative method produces approximately correct results, it is very unstable, especially when a complex fault is present. When multiple interactions occur between particle-pairs, the algorithm does not converge, in which case the error in energy may exceed 100%.

As shown previously, the Cundall approach is stable, but the value of the joint stiffness K_s plays an important role in the static–dynamic behaviour. The joint stiffness K_s represents the effective shear rigidity of particles in static frictional contact when subjected to shear forces. An infinite value of K_s will cause particles to become rigid (like particles in the lattice solid model). Hence, when large values of K_s are used with the Cundall approach, the results should become similar to those obtained with the lattice solid model.

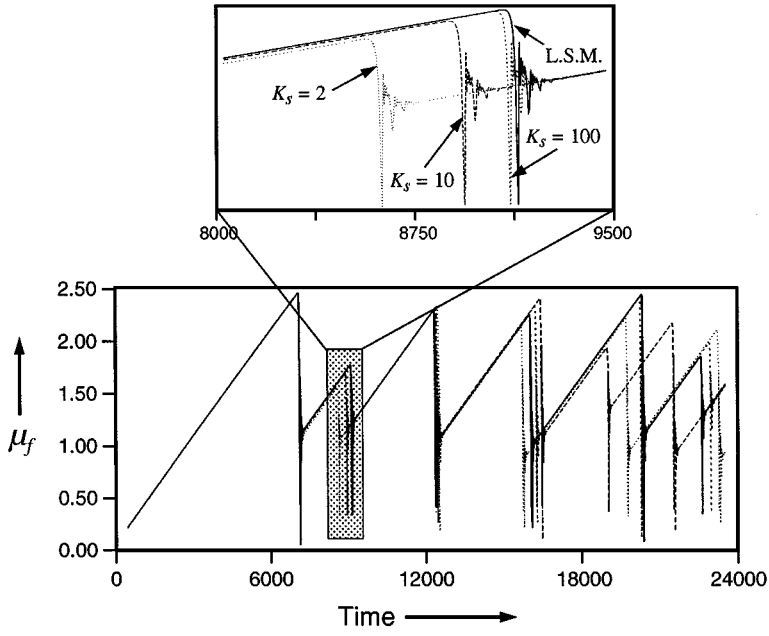

FIG. 21. Plot of the fault friction using the lattice solid model approach (solid line) and the Cundall approach for a value of $K_s = 2.0$ (dotted line), $K_s = 10.0$ (dashed line), and $K_s = 100.0$ (fine dashed line).

The purpose of the following numerical experiments is to determine the value of K_s that should be used to obtain results similar to those obtained with the lattice solid model, and the computational cost. These experiments used the setup described in Fig. 17. Different values of the joint stiffness K_s ranging from 0.1 to 100 are used and the time step increment is chosen according to Eq. (38). The computational cost (CPU time) and accuracy of the results are compared with the results obtained using the lattice solid model.

As the value of the joint stiffness becomes larger, results obtained using the Cundall approach become more like those obtained with the lattice solid model approach (Fig. 21).

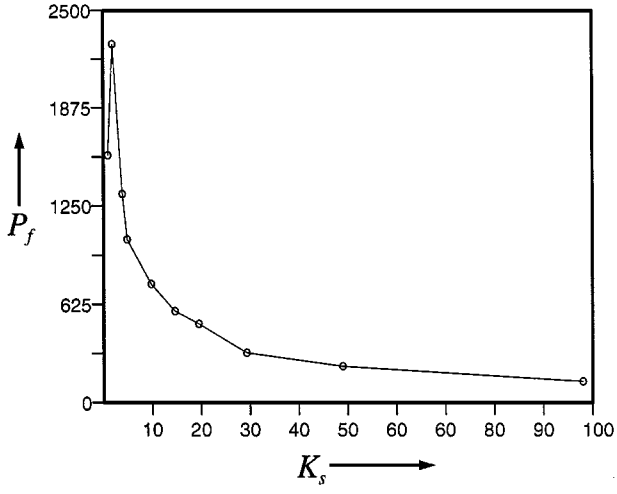

FIG. 22. Precision factor of the Cundall approach plotted as a function of the joint stiffness K_s.

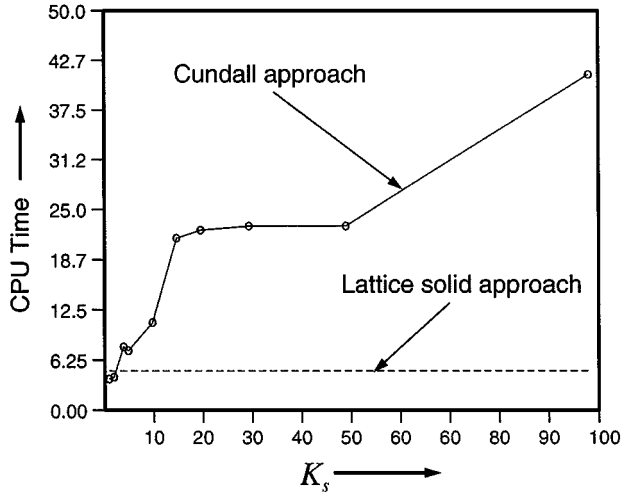

FIG. 23. Comparison between the Cundall approach and the lattice solid model approach. The computational time is plotted as a function of the joint stiffness K_s.

Figure 22 shows the precision factor between the Cundall approach and the lattice solid model approach computed as

$$P_f = \frac{(\varepsilon_h)_{\text{Cundall}}}{(\varepsilon_h)_{LSM}}, \tag{A.2}$$

where the error in the heat energy using the lattice solid model ($(\varepsilon_h)_{LSM}$) is chosen as the reference and is equal to 0.01% for this numerical experiment. This precision factor represents the amount of slip that occurs when particles are locked by static friction (caused by the shear deformation of the particle) and should converge to 1 as the particle becomes more rigid. Figure 23 shows the CPU time using the Cundall approach for different values of K_s compared with our method.

For a value of K_s greater than 100, where the precision factor is less than 200 (i.e., the heat generated when the contact is static is less than 2%), the frictional stress becomes almost equal to the stress computed using the lattice solid model (Fig. 21). In this case (for a simple fault) the Cundall approach is approximately 40 times slower. If a more complex fault is specified, the error becomes larger, and the value of K_s required to obtain similar results becomes larger. Consequently, when "rigid" shear constraint is used, the Cundall approach becomes excessively costly.

ACKNOWLEDGMENTS

The research was funded by the Australian Research Council. Supplementary funding was provided by The University of Queensland (UQ), the sponsor of QUAKES. Principle computations were made using the QUAKES 12 processor, Silicon Graphics Origin 2000. Supplementary and seed computations were made using respectively UQ's Power Challenge, the QUAKES Power Challenge; and the CM-5 of the French National Centre for Parallel Computing in the Earth Sciences (CNCPST). We thank P. A. Cundall for an insightful, comprehensive, and constructive review.

REFERENCES

1. K. Aki and P. G. Richards, *Quantitative Seismology: Theory and Methods* (Freeman, San Francisco, 1980), p. 4.
2. M. P. Allen and D. J. Tildesley, *Computer Simulations of Liquids* (Oxford Univ. Press, New York, 1987).
3. J. N. Brune, S. Brown, and P. A. Johnson, Rupture mechanism and interface separation in foam rubber models of earthquakes: A possible solution to the heat flow paradox and the paradox of large ovethrusts, *Tectonophysics* **218**, 59–56 (1993).
4. S. R. Brown and C. H. Scholz, Broad bandwidth study of the topography of natural rock surfaces, *J. Geophys. Res.* **89**, 3051–3058 (1985).
5. N. H. Christ, R. Friedberg, and T. D. Lee, Random lattice field theory, *Nucl. Phys. B* **202**, 89–125 (1982).
6. P. A. Cundall and O. D. L. Strack, A discrete numerical model for granular assemblies, *Géotechnique* **29**, 47–65 (1979).
7. F. Donzé, P. Mora, and S. A. Magnier, Numerical simulation of faults and shear zones, *Geophys. J. Int.* **116**, 46–52 (1993).
8. R. Hart, P. A. Cundall, and J. Lemos, Formulation of a three-dimensional distinct element model, II, *Int. J. Rock Mech. Min. Sci. Geomech.* **25**, 117–125 (1988).
9. A. H. Lachenbruch and A. McGarr, Stress and heat flow, in *U.S. Geological Survey Organisation Professional Paper 1515* (U.S. Govt. Printing Office, Washington DC, 1990), Chap. 10, pp. 261–277.
10. A. H. Lachenbruch and J. H. Sass, *J. Geophys. Res.* **97**, 4995–5015 (1992).
11. P. S. Lomdahl, P. Tamayo, N. Gronbech-Jensen, and D. M. Beazley, G-flops molecular dynamics on the Connection Machine 5, in *Proceedings, SuperComputing 93, Portland, Oregon, November 1993* (IEEE Comput. Soc. Press, Los Alamitos, CA, 1993).
12. P. S. Lomdahl, D. M. Beazley, P. Tamayo, and N. Gronbech-Jensen, Multimillion particle molecular dynamics on the CM5, *Int. J. Mod. Phys. C* **4**, 1075–1084 (1993).
13. H. J. Melosh, *Nature* **379**, 601–606 (1996).
14. P. Mora, A lattice solid model for rock rheology and tectonics, *Seismic Simulation Project Tech. Rep.* **4**, 3–28 (1992). [Institut de Physique du Globe, Paris]
15. P. Mora and D. Place, A lattice solid model for the nonlinear dynamics of earthquakes, *Int. J. Mod. Phys. C* **4**, 1059–1074 (1993).
16. P. Mora and D. Place, Simulation of the frictional stick-slip instability, *Pure Appl. Geophys.* **143**, 61–87 (1994).
17. P. Mora and D. Place, Simulation of stick-slip: Effect of intrinsic friction, in *AGU 1995 Fall Meeting Prog. and Abstracts* (published as suppl. to *EOS*, Nov. 12, 1995).
18. P. Mora and D. Place, Numerical simulation of earthquake faults with gouge: Towards a comprehensive explanation for the heat flow paradox, *J. Geophys. Res.* **3**, 21,067–21,089 (1998).
19. P. Mora and D. Place, The weakness of earthquake faults, *Geophys. Res. Lett.* **26**, 123 (1999).
20. D. Pisarenko and P. Mora, Velocity weakening in a dynamical model of friction, *Pure Appl. Geophys.* **142**, 447–466 (1994).
21. D. Place and P. Mora, The atomic lattice solid algorithm, *Seismic Simulation Project Tech. Rep.* **5**, 37–41, (1993). [Institut de Physique du Globe, Paris]
22. D. Place and P. Mora, Large scale simulation of the physics of earthquakes, in *AGU 1995 Fall Meeting Prog. and Abstracts* (published as suppl. to *EOS*, Nov. 12, 1995).
23. D. Place and P. Mora, The lattice solid model: Towards large scale simulations, *QUAKES Tech. Rep.* **3**, 247–270 (1998). [The University of Queensland]
24. D. Place and P. Mora, Numerical simulation of localisation phenomena in a fault zone, *QUAKES Tech. Rep.* **3**, 227–246 (1998). [The University of Queensland]
25. M. Winter, D. Place, and P. Mora, Incorporation of particle scale rotational dynamics into the lattice solid model, *EOS Trans. Am. Geophys. Union* **78**, No. 46, F477 (1997).